ISSN 0915-633X

NATIONAL INSTITUTE FOR FUSION SCIENCE

Neoclassical Transport Analysis in the Banana Regime on Large Helical Device (LHD) with the DKES Code

Y. Ogawa, T. Amano, N. Nakajima, Y. Ohyabu, K. Yamazaki
S. P. Hirshman, W. I. van Rij and K. C. Shaing

(Received – Aug. 20, 1991)

NIFS-108 Sep. 1991

RESEARCH REPORT
NIFS Series

NAGOYA, JAPAN

Neoclassical transport analysis in the banana regime on Large Helical Device (LHD) with the DKES code

Y. Ogawa, T. Amano, N. Nakajima, Y. Ohyabu, K. Yamazaki,
National Institute for Fusion Science
Nagoya, 464-01, Japan
and
S.P. Hirshman, W.I. van Rij and K.C. Shaing
Oak Ridge National Laboratory
Oak Ridge, Tennessee 37831, U.S.A.

Abstract

Neoclassical transport in the banana regime has been analyzed with the DKES (Drift Kinetic Equation Solver) code for the Large Helical Device (LHD). It is found that in a $1/\nu$ regime, diffusion coefficients change by one order of magnitude for various configurations of LHD (-0.2 m $\leq \Delta \leq 0$ m, $0\% \leq Bq \leq 200\%$, $-0.1 \leq \alpha \leq 0.1$), depending on the structure of the helical magnetic ripple. The neoclassical transport calculated with the DKES code is quantitatively in good agreement with multi-helicity theory formulated by Shaing and Hokin. Incorporating the multi-helicity effect into the diffusion coefficient, we have proposed an interpolation formula between the $1/\nu$ and ν regimes. When the ion temperature is increased at a fixed density of $n = 10^{20}$ m^{-3}, the ions undergo a transition from $1/\nu$ neoclassical transport to the ν regime when their temperature T_i becomes > 3 keV with radial electric potential $e\phi$ comparable to the ion temperature ($e\phi/T_i \approx 1$). For the optimized configuration ($\Delta = -0.2$ m, $Bq = 100\%$), the ion thermal diffusivity χ_i has a maximum value of $\chi_i \approx 3.5$ m^2/s at a minor radius of $r/a \approx 0.5$. The bootstrap current has been also studied, and the results have been comprehensively compared with the theory. At the collisionless limit with a moderate radial electric potential of $e\phi/T_i \approx 1$, the DKES calculations evaluated for various configurations of LHD have supported the theoretical formula given by Shaing and Callen. At the collision frequency between the plateau and the banana regimes, where the analytic theory is not applicable, the bootstrap current might become larger than in the collisionless limit (by a factor of about two), depending on the radial electric field.

Keywords : Large Helical Device (LHD), neoclassical transport, banana regime, DKES code, thermal diffusivity, bootstrap current, multi-helicity effect

(I) Introduction

It has been recognized in helical systems that neoclassical transport plays a crucial role in the confinement of a reactor-grade collisionless plasma. Compared with tokamak systems, however, the analysis of the neoclassical transport in a helical system is not so straightforward, because of the three-dimensional (3-D) sophisticated magnetic field configuration. Theoretically, some formulae for neoclassical transport coefficients have been derived for each collisionality regime with appropriate assumptions[1-3]. Simulations with a Monte Carlo technique are useful as well, and some literature has analyzed the neoclassical transport in helical systems[4-8].

Hirshman et al. have developed a computer code, DKES (Drift Kinetic Equation Solver), to solve the drift kinetic equation in 3-D helical magnetic configurations, and have analyzed the neoclassical transport for the ATF (l=2,m=12) and TJ-II (Heliac) devices[9,10]. This code is also powerful in advancing theoretical efforts to develop the neoclassical transport formula in helical systems, and Crume et al. have established a new scaling for the neoclassical transport in the ν-regime[11]. In addition, the analysis of the bootstrap current has been done, since the off-diagonal terms of the transport matrix are also calculated with this code[12].

The Wendelstein VII-AS group has made comprehensive comparisons between experimentally observed thermal diffusivities and those calculated by DKES[13]. Recently, applications of the DKES code for CHS (l=2, m=8) experiments have been done[14]. In ATF experiments, the control of the bootstrap current with the quadrupole magnetic field has been clearly demonstrated, and these experimental results have been in good agreement with DKES calculations[15].

Concerning the Large Helical Device (LHD)[16], the construction of which was initiated in 1991, many computations of the neoclassical transport have been carried out from the viewpoint of single particle orbits[17] and bootstrap current[18]. To predict plasma parameters for LHD, two-dimensional equilibrium-transport simulations have been carried out, in which an empirical scaling and drift wave turbulence models have been employed, in addition to the neoclassical transport[19].

In this paper we study the neoclassical transport in the LHD configuration with the DKES code. Theoretically, the tailoring of the helical ripples (like a σ-optimization) makes a great reduction of the neoclassical transport[20,21]. The LHD has a great potential to realize various plasma configurations, by adjusting the currents in the helical coils (with three layers) and poloidal coils (with three pairs). Multi-helicity effects have been carefully studied for these configurations from the viewpoint of reducing the neoclassical transport.

In section II, the specification of LHD is presented. In section III, the thermal diffusivities calculated with the DKES code for various LHD configurations are presented, and the effect of the multi-helicity on the neoclassical transport coefficients is extensively studied. The bootstrap current is analyzed in section IV. Section V summarized the results.

(II) Specification of the Large Helical Device (LHD)

The Large Helical Device (LHD) is an l=2 heliotron/torsatron-type helical machine with the superconducting helical coils of an m=10 pitch number. Specifications for LHD are tabulated in Table I, in which the latest parameters are presented[16]. A few parameters employed in the transport analysis considered in this paper are slightly different from these specified values. Values in brackets in Table I are used in the present analysis.

A pair of continuous helical coils consists of three layers, and coil currents for each layer are fed independently. This makes it possible to change the pitch parameter, defined by $\gamma=(a_c/R_c)*(m/l)$, where R_c and a_c are major and minor radii of helical coils, respectively. There are also three pairs of poloidal field coils, called IV, OV and IS coils. A vertical field component is mainly produced through two pairs of them (IV and OV coils), shifting the plasma column horizontally. Another pair (IS coil) is used to control the quadrupole field component, making an elliptical deformation of the plasma cross section. Typically the design of these poloidal field coils makes it possible to change the plasma position and the shape for full field operations in the following regime:

Plasma position : $-0.3\ \mathrm{m} \le \Delta \le 0\ \mathrm{m}$
Quadrupole field : $0\% \le Bq \le 200\%$,

where Bq = 100% means the complete cancellation of the quadrupole field component produced by the helical coils and corresponds approximately to a toroidally averaged plasma shape with a circular cross section. In contrast, Bq = 0%(200%) corresponds to a vertically (horizontally) elongated plasma.

In designing the helical field coils for LHD, we have considered the pitch modulation from the viewpoints of bulk plasma confinement, high energy particle orbits, MHD stability and divertor design. The pitch modulation parameter α is defined by $\theta = (m/l)*\phi+\alpha*\sin\{(m/l)*\phi\}$ (θ and ϕ are poloidal and toroidal angles, respectively). Taking engineering constraints into account, the performance of LHD plasmas has been studied for pitch modulation parameters of $-0.1 \leq \alpha \leq 0.2$. The final design corresponds to $\alpha = 0.1$[19].

(III) Transport analysis with the DKES code

The DKES code was developed by Hirshman et al.[9,10] to calculate neoclassical diffusion coefficients for 3-D magnetic geometry. In this code, the drift kinetic equation is numerically solved in phase space, where a perturbed distribution function is expanding with Legendre polynomials in pitch angle of the velocity space, and with Fourier modes in poloidal and toroidal components on the given magnetic surface. With respect to the Coulomb collision operator, only the pitch angle scattering term is retained, and the energy diffusion term and the momentum conservation between electrons and ions are neglected for the simplification of the code. The application of the DKES code is, therefore, valid in the long mean free path, namely the banana ($1/\nu$ and ν) regimes, where trapping/detrapping effects govern the neoclassical transport. If the DKES code were to be applied for collisional plasmas, it would be necessary to retain the effects of energy diffusion and momentum conservation.

In the DKES code, three components of the transport matrix ((1,1), (3,1) and (3,3) components) are calculated as functions of two independent parameters (one is the mean free path at a fixed particle energy , $(\nu/v)^{-1}$, and another is the radial electric field divided by the particle velocity E_r/v, where ν, v and E_r are the collision frequency, particle velocity and radial electric field, respectively). The upper and lower values of these three components are obtained by a variational principle. Other components of the transport matrix are derived from these three values. Since DKES gives the transport coefficients at a fixed particle energy, the transport coefficients for a plasma with a Maxwellian distribution function are calculated by integrating DKES data weighted by a Maxwellian as follows:

$$D_{ij} = \frac{v_{th}}{\sqrt{\pi}}\left(\frac{Bv_{th}}{\Omega}\right)^2 \int_0^\infty E^{i+j}\exp(-E)D_{E1}dE \tag{1}$$

where (i,j) = 1 or 2, and $v_{th} = (2T/m)^{1/2}$, $\Omega = ZeB/m$, B is the strength of the magnetic field, and D_{E1} is the data calculated with the DKES code.

To get a sufficient convergence in computation, we have employed up to 150 Legendre polynomials P_l, and up to 300 Fourier modes (m,n).

(III.1) Configuration study

In Fig. 1, values of D_{E1} calculated with the DKES code are plotted as a function of the inverse of the mean free path ($CMUL$=ν/v) for various radial electric fields ($EFIELD=E_r/v$), where a plasma equilibrium shifted 0.2 m inward is employed. The diffusion coefficients are obtained with sufficient accuracy for the parameter regime of $CMUL \geq 10^{-5}$, where the bound of the upper and lower limits is represented with an error bar. At $CMUL \leq 10^{-6}$, we have extrapolated the diffusion coefficients by assuming a 1/ν or ν variation for D_{E1}. This is necessary because the convergence of the code with respect to the Legendre-Fourier basis is slow at these low collisionality regimes.

The diffusion coefficients with a Maxwellian plasma can be deduced by integrating the D_{E1} data along the path shown in Fig. 1. First, we study the neoclassical transport for the mono-energy cases, in relation to various LHD magnetic configurations. Since our main interest is transport in the 1/ν or ν regime, the collision frequency is chosen to be $CMUL = 3\text{x}10^{-5}$ or 10^{-4}, where the neoclassical transport is observed to be in the banana (1/ν or ν) regime.

Single-helicity

The neoclassical transport for a single-helicity configuration is theoretically given[3,11] as :

$$\begin{array}{llll} 1/\nu \text{ regime} & : & D_{E1} \propto \varepsilon_t^2 \varepsilon_h^{3/2}\,, & (2) \\ \nu \text{ regime} & : & D_{E1} \propto \varepsilon_t \varepsilon_h^{1/2}\,, \text{ or} & (3a) \\ & : & D_{E1} \propto \varepsilon_t^{3/2}\,, & (3b) \end{array}$$

where the magnetic field is represented by $B/B_0 = 1 - \varepsilon_t\cos(\theta) + \varepsilon_h\cos(l\theta - m\phi)$. Especially in the ν regime, two scalings with the toroidal (ε_t) and helical (ε_h) ripples are proposed. We have calculated the diffusion coefficients for various toroidal and helical ripples, and results are shown in

Fig. 2. The radial electric field, as denoted by the *EFIELD* parameter, was chosen to be $EFIELD = 10^{-6}$ ($EFIELD > 3\times10^{-3}$) in the $1/\nu$ regime (the ν regime). These data show that in the $1/\nu$ regime, the diffusion coefficient is proportional to $\varepsilon_t^2 \varepsilon_h^{3/2}$, as given in eq. (2). In the ν regime, two scalings are also plotted in Fig. 2, and our data support the scaling of eq. (3b) rather than that of eq.(3a), although variation of the data is not so large. Since the scaling of eq.(3b) was previously established with the DKES calculations for l=2/m=12 ATF machine parameters[11], it is not surprising that our results for l=2/m=10 LHD parameters are in agreement with this scaling.

Radial electric field

In Fig. 3 the diffusion coefficients are plotted against the radial electric field for two typical magnetic configurations:

(a) Δ = - 0.2 m, Bq = 100%,
(b) Δ = 0 m, Bq = 0%,

where case (a) is a circular plasma with an inward shift of 0.2 m, and case (b) is a vertically elongated one with no shift. Fourier components of the magnetic field $|B|$ for these configurations are shown in Fig. 4, in which the magnetic field ripple along the field line at a minor radius of $r/a \approx 0.5$ is also presented. These two configurations are similar with respect to the dominant single-helicity components (ε_t and ε_h), as shown in Table II. Other components of the helical ripple are, however, quite different between these cases. In case (a), the helical ripple is localized at a high-field region, while in case (b) the deep helical ripple exists in a low-field region. From these field structures, it is predicted[20] that the neoclassical diffusion coefficients in case (a) are smaller than those of case (b).

The multi-helicity effect makes a great difference in the $1/\nu$ regime, as shown in Fig. 3. When the radial electric field is increased, the diffusion coefficient begins to decrease, approximately in proportion to $1/E_r^2$. It appears that as the radial electric field is increased, the difference between two cases becomes smaller, and the D_{E1} values with the multi-helicity components seem to converge to those with only the single-helicity one. This result will also support the scaling of eq. (3b); i.e., in the ν regime the helical ripple structure with the multi-helicity components does not affect the neoclassical transport so much.

Various configurations

As discussed in section II, many different magnetic configurations can be produced with the LHD device. Here we have calculated the neoclassical transport for various configurations which can be realized in the LHD. The diffusion coefficients in the $1/\nu$ and ν regimes are presented in Figs. 5-7 as a function of the plasma minor radius. Plasma parameters are assumed to be uniform in radius (the same collision frequency is used for each minor radius). The magnetic field structure along the field line around $r/a \approx 0.5$ is represented for each configuration, as well.

As shown in Fig. 5, the inward shift of the plasma column improves the confinement in the $1/\nu$ regime. It is shown in Fig. 6 that the superposition of the quadrupole magnetic field around Bq = 100% is effective in reducing the diffusion coefficient. The improvement of case (a) configuration, compared with the case (b), is accounted for by these two factors. Figure 7 indicates that a positive pitch modulation of the helical coil is not desirable from the viewpoint of the neoclassical transport. These characteristics of the diffusion coefficient in the $1/\nu$ regime are reasonably accounted for, if the magnetic field ripple along the field line, as shown in each figure, is taken into consideration. The idea of reducing neoclassical transport by controlling the plasma position and shape was originally proposed for LHD in ref.[17].

Shaing and Hokin have developed a theory to account for the multi-helicity effect on neoclassical transport in the $1/\nu$ regime[21]. Here we have compared this theory with the numerical results for these various configurations. Shaing and Hokin derived the neoclassical flux, including the multi-helicity effect in the $1/\nu$ regime, in which the diffusion coefficient depends on the magnetic field structure factorized as follows:

$$F = \int_0^{2\pi} d\theta \ \varepsilon_H^{3/2} \left[G_1 \left(\frac{\partial \varepsilon_T}{\partial \theta} \right)^2 - 2G_2 \frac{\partial \varepsilon_T}{\partial \theta} \frac{\partial \varepsilon_H}{\partial \theta} + G_3 \left(\frac{\partial \varepsilon_H}{\partial \theta} \right)^2 \right] \quad (4)$$

where G_1=16/9, G_2=16/15, G_3=0.684, and $\varepsilon_T=\varepsilon_t\cos\theta + \varepsilon_d\cos l\theta$, $\varepsilon_H=(C^2+D^2)^{1/2}$, $C=\varepsilon^{(0)}+(\varepsilon^{(+1)}+\varepsilon^{(-1)})\cos\theta + (\varepsilon^{(+2)}+\varepsilon^{(-2)})\cos 2\theta$, and $D=(\varepsilon^{(+1)}-\varepsilon^{(-1)})\sin\theta + (\varepsilon^{(+2)}-\varepsilon^{(-2)})\sin 2\theta$. We introduce the correction factor due to the multi-helicity effect, defined as;

$$C_m = F_m \,/\, F_s\,, \tag{5}$$

where F_s and F_m are values calculated with eq. (4) for single- and multi-helicity magnetic configurations, respectively. This correction factor is evaluated for the various configurations shown in Figs. 5-7, and the diffusion coefficients are plotted in Fig. 8 as functions of two scaling parameters ($\Lambda_s = \varepsilon_t^2 \varepsilon_h^{3/2}/B_0^2$ and $\Lambda_m = C_m \varepsilon_t^2 \varepsilon_h^{3/2}/B_0^2$), where magnetic field structures of -0.2 m $\leq \Delta \leq 0$ m, $0\% \leq Bq \leq 200\%$ and $-0.1 \leq \alpha \leq 0.1$ are employed. We can see that the diffusion coefficient has a variation of one order of magnitude for similar $\Lambda_s = \varepsilon_t^2 \varepsilon_h^{3/2}/B_0^2$ values (open circles). This suggests that the evaluation of the diffusion coefficient with only the single-helicity mode is not accurate for these various configurations. When the correction factor C_m due to the multi-helicity effect is introduced into the scaling, the diffusion coefficients are clearly proportional to $\Lambda_m = C_m \varepsilon_t^2 \varepsilon_h^{3/2}/B_0^2$ (solid circles). We conclude that the correction factor defined by eq. (5) is reasonably applicable for these various configuration of the LHD.

In the ν regime, the diffusion coefficients are 2-3 orders of magnitude lower than those in the $1/\nu$ regime for all configurations. It appears also that the differences in the diffusion coefficients observed in the $1/\nu$ regime for the various magnetic configurations becomes smaller, or disappear, in the ν regime. This characteristics may also support the scaling given by eq. (3b) in the ν regime rather than that of eq. (3a).

Interpolation formula

With respect to the diffusion coefficients in the $1/\nu$ regime, we have found in the previous section that the correction due to the multi-helicity effect, introduced by Shaing and Hokin, is reasonably applicable for a wide range of magnetic configurations in the LHD. We have also observed that in the ν regime the thermal diffusivity has a very weak dependence on the helical ripple, supporting the formula given by eq. (3b) rather than eq. (3a).

An interpolation formula for the thermal diffusivity between the 1/ν and ν regimes has been proposed by Crume et al. for the single-helicity model[11]. Here we have incorporated the multi-helicity effect into the interpolation formula as follows:

$$Q=\varepsilon_t^2\varepsilon_h^{1/2}v_d^2 nT\int_0^\infty E^{7/2}\exp(-E)\frac{\nu_h(E)(A_1+EA_2)}{\omega^2(E)}dE \quad , \qquad (6a)$$

$$\omega^2(E)=1.5\sqrt{\varepsilon_t/\varepsilon_h}\,\Omega_E^2+3\nu_h^2(E)/C_m \quad , \qquad (6b)$$

where $v_d=T/(ZerB)$, $\nu_h(E)=\nu(E)/\varepsilon_h$, $A_1=n'/n-1.5T'/T-eE_r/T$, $A_2=T'/T$, $\Omega_E=E_r/(rB)$. The first and second terms in $\omega^2(E)$ correspond to the diffusion coefficients in the 1/ν and the ν regimes, respectively, and C_m is the correction factor due to the multi-helicity effect, defined in eq. (5). This interpolation formula can be rewritten as

$$D_m=D_s\frac{R_C+1}{R_C+1/C_m} \quad , \qquad R_C=\frac{1.5\sqrt{\varepsilon_t/\varepsilon_h}\,\Omega_E^2}{3\nu_h^2(E)} \quad , \qquad (7)$$

where D_m (D_s) denotes the diffusion coefficient for the multi- (single-) helicity case, and R_c is the ratio of the diffusion coefficients for the 1/ν and the ν regimes. Equation (7) gives $D_m=C_m*D_s$ as the limit of R_c --> 0 (i.e., in the 1/ν regime), and $D_m=D_s$ for R_c >> 1 in the ν regime. Figure 9 shows the diffusion coefficients interpolated by eq. (7) compared with the DKES data for single- and multi-helicity cases. In the 1/ν regime (smaller radial electric field case; $R_c < 1$), the correction due to multi-helicity is well approximated. At relatively large electric field ($R_c > 1$), however, the interpolation is not as accurate, although the difference between single- and multi-helicities is small.

(III.2) Thermal diffusivity for typical cases

For the two typical configurations of the LHD listed in Table II, we have evaluated ion and electron thermal diffusivities with the DKES code. Thermal diffusivity $\chi_{i,e}$ is calculated by integrating D_{EI} values along the path shown in Fig. 1 by a broken line (weighted by a Maxwellian distribution function). The upper bound of the energy integration is extended to $E_{max} = 18.4T_{i,e}$, since the maximum of the integrand in eq. (1) appears around an energy of $E \approx 6T_{i,e}$ in the 1/ν regime.

To simulate plasma heating experiments, we have calculated the thermal diffusivity as a function of the plasma temperature at a fixed density. In Figs. 10 and 11, ion and electron thermal diffusivities χ_i and χ_e evaluated at a minor radius $r/a \approx 0.5$ are presented as a function of the collision frequency, where the plasma density is fixed to be $n = 10^{20}$ m^{-3}. The radial electric field is converted into the potential ϕ, assuming the relation $E_r = -e^*\mathrm{grad}\phi = -e\phi/a_\phi$, and the value of $e\phi/T_{i,e}$ is kept constant for each curve, according to the change of the collision frequency.

It is shown for ions and electrons that $\chi_{i,e}$ values are proportional to $T_i^{7/2}$ in the 1/ν regime, as predicted by theory. The electron thermal diffusivity χ_e increases monotonically with T_e up to $T_e = 10$ keV, while the ion transport enters the ν regime at $T_i = 2$-3 keV. The peak value of χ_i at the transition from the 1/ν to the ν regime is significant, because it must be overcome to achieve a high-temperature plasma (if the anomalous transport is suppressed at a sufficiently low level, just like an H-mode in tokamaks [22]). As a consequence of the multi-helicity effect, the peak value is quite different between two cases; $\chi_i(peak) \approx 3.5$ m^2/s in case (a) and $\chi_i(peak) \approx 20$ m^2/s in case (b), if $e\phi/T_i = 1$. Figure 12 plots the peak values of the ion thermal diffusivity $\chi_i(peak)$ as a function of the corresponding ion temperature for various densities, where the radial electric field of $e\phi/T_i=1$ is assumed. The range of the ion temperature with $\chi_i > 0.9\chi_i(peak)$ is also presented. The ion thermal diffusivity for case (a) is about 5 - 10 times lower than for case (b).

At the collisionless limit of the 1/ν and the ν regimes, eq. (6a) yields the ion thermal diffusivity as:

1/ν regime : $$\chi_i(1/\nu) = \frac{C_{1/\nu}\varepsilon_t^{2}\varepsilon_h^{3/2}v_d^{2}}{3\nu_{th}^{i/i}} \qquad (8a)$$

$$\nu \text{ regime}: \qquad \chi_i(\nu) = \frac{C_\nu \varepsilon_t^{3/2} v_d^2 \nu_{th}^{i/i}}{1.5\Omega_E^2} \tag{8b}$$

where $C_{1/\nu}$ =585.1 and C_ν = 2.711, and $\nu_{th}^{i/i}$ is the ion-ion collision frequency at the thermal energy. Equating eqs. (8a) and (8b), an ion temperature which gives a peak value of χ_i is obtained:

$$T_i(\mathrm{keV}) = C_T \left\{ \frac{r^2 B^2}{\varepsilon_t^{1/2} \varepsilon_h^{3/2} C_m} \cdot \frac{a_\phi^2 n_{20}^2}{(e\phi / T_i)^2} \right\}^{\frac{1}{5}} \tag{9}$$

where C_T = 0.7535 and n_{20} is a density normalized by 10^{20} m^{-3}. Arrows in Fig. 12 indicate the ion temperature calculated by eq. (9), showing good agreement with the DKES calculations.

Another interesting point is that the transition region from the $1/\nu$ to the ν regime is relatively wide, as shown in Fig. 10; e.g., the collision frequency regime with $\chi_i > 0.9\chi_i(peak)$ is 2 keV < T_i < 4 keV for n = $10^{20}m^{-3}$ in case (a). This means that in heating experiments an ion must experience a wide range of the temperature with a relatively large ion thermal diffusivity ($\chi_i > 0.9\chi_i(peak)$), making it difficult for ions to enter the low diffusivity regime.

(IV) Analysis of the bootstrap current

Compared with axisymmetric tokamaks, helical systems reveal some interesting features of the bootstrap current. In helical systems, it is possible to control the bootstrap current with external coils. Since the bootstrap current might modify or destroy the vacuum magnetic surface, the control and reduction of the bootstrap current are indispensable in helical systems.

The analytical treatment of the bootstrap current in helical systems is more sophisticated than in tokamaks. Introducing some assumptions in the analysis, formulae for the bootstrap current have been recently derived in the banana [23,24] and the plateau [25] regimes. By comparing numerical data calculated with the DKES code, the validity of these formulae has been intensively studied in ref. [12], in which the parameters of ATF(l=2,m=12) with a single helicity have been employed. In ref. [26], the control and suppression of the bootstrap current using a poloidal coil system have been demonstrated. For the LHD, Nakajima et al. have quantitatively evaluated the bootstrap current with these formulae and discussed the reduction of the bootstrap current by changing plasma shapes and positions with poloidal coils[18]. Here we have analyzed the bootstrap current with the DKES code for the LHD and examined the validity of the theoretical formulae, especially with respect to the multi-helicity effect.

In the banana regime, Shaing and Callen derived the formula for the bootstrap current as follows [23] :

$$< J_{bs}B > = 2.95\frac{f_t}{f_c}G_{bs}\left\{a_1(T_e+T_i)\frac{dn}{dV}+a_2 n\frac{dT_i}{dV}+a_3 n\frac{dT_e}{dV}\right\}, \tag{10a}$$

and

$$f_c = \frac{3}{4}\frac{< B^2 >}{B^2_{max}}\int_0^1\frac{\lambda d\lambda}{< g_1 >}, \qquad f_t = 1 - f_c$$

$$G_{bs} = \frac{1}{f_t}\left[< g_2 > - \frac{3}{4}\frac{< B^2 >}{B^2_{max}}\int_0^1\frac{< g_4 >}{< g_1 >}\lambda d\lambda\right], \tag{10b}$$

where J_{bs} and B are the bootstrap current and the magnetic field strength, respectively, and <.....> denotes the magnetic surface average. V is the plasma volume, and n, T_i and T_e are density and ion/electron temperatures, respectively. The numerical coefficients are a_1 = 0.554, a_2 = -0.0941 and a_3 = 0.1404. The fraction of trapped (circulating) particles is represented by f_t (f_c), G_{bs} is the geometric factor, and other parameters are given in ref. [18].

A specific character of this formula is that the coefficient G_{bs} given by eq. (10b) is a function only of the magnetic field structure and is independent of collision frequency ν and radial electric field E_r. In deriving this formula, a proper radial electric field is introduced a priori, to smear out the boundary between trapping and detrapping in the velocity space. As a consequence, this formula is applicable at the collisionless limit with the finite radial electric field, $e\phi/T_i \approx 1$.

The DKES code can compute the off-diagonal term of the transport matrix. The D_{E3} term calculated with the DKES code corresponds to the bootstrap current. (This term does not give the net bootstrap current, because momentum conservation is ignored in solving the drift kinetic equation.)

First, we have examined the validity of the assumptions employed in deriving eq. (10). Figure 13 shows D_{E3} as a function of the collision frequency for various radial electric fields, where data corresponding to a tokamak configuration (all helical ripples are set to be zero) are also plotted. As the collision frequency decreases, the bootstrap current increases in the banana regime and seems to saturate at the collisionless limit. In addition, this saturation level seems to be insensitive to the radial electric field, if a radial electric field($e\phi/T \approx 1$) is introduced. In Fig. 14 the D_{E1} and D_{E3} terms are replotted as a function of the radial electric field. It is clearly seen that the D_{E3} term has a plateau around $e\phi/T \approx 1$. These results calculated with the DKES code, thus, support the conclusion that the bootstrap current is independent of the collision frequency and is insensitive to the radial electric field around $e\phi/T \approx 1$.

At the collision frequency corresponding to the transition between the plateau and the banana regimes, the analytic theory is not applicable. We can see from Fig. 13 that the bootstrap current does not monotonically increase as the collision frequency is decreased and is very sensitive to the radial electric field in this transition regime. In particular, the bootstrap current in the transition regime can become larger than that in the collisionless limit, when the radial electric field is relatively weak ($e\phi/T <<$ 1). This implies that the bootstrap current calculated with eq. (10) does not give the upper limit of the induced bootstrap current for $e\phi/T << 1$.

Next, the bootstrap current calculated with the DKES code has been compared with theoretical values. Figure 15 shows the bootstrap current as a function of the radial electric field for different plasma minor radii: i.e., for different magnetic field ripples. We can see that around $e\phi/T \approx 1$ the bootstrap current becomes insensitive to the radial electric field, as discussed previously. The bootstrap currents, normalized by that of the equivalent tokamak, are plotted in Fig. 16 as a function of the plasma minor radius for two different configurations. The theoretical values are calculated with eq. (10), and the values around $e\phi/T \approx 1$, shown in Fig. 15, are selected from the DKES data. It is confirmed with Fig. 16 that the agreement between theory and DKES results is very good not only for the single-helicity case but also for the multi-helicity case, although the difference is slightly larger in the multi-helicity of case (a). We can also see that the amplitude of the bootstrap current in the LHD case is about 2 - 5 times lower than that in the equivalent tokamak.

It has been demonstrated, theoretically and experimentally, that the quadrupole field is effective in controlling the bootstrap current[26,27]. We have examined the dependence of the bootstrap current on the quadrupole field. Figure 17 shows the bootstrap current as a function of the quadrupole field component Bq. We can see the possibility of reducing the bootstrap current by a factor of two, by elongating the plasma cross section vertically.

We conclude that the assumptions employed in deriving eq. (10) are valid and the formula for the bootstrap current is applicable for various configurations (single- and multi-helicities). We should, however, remark that at the transition collision frequency from the plateau to the banana regime, the bootstrap current might become larger than that in the collisionless limit within a factor of around two, at least for weak radial electric fields.

(V) Summary

Neoclassical transport in the banana regime has been analyzed with the DKES code for LHD. We have studied the thermal diffusivity for various configurations of LHD, by changing the plasma position (-0.2 m $\leq \Delta \leq 0$ m), the quadrupole field ($0\% \leq Bq \leq 200\%$) and the pitch modulation ($-0.1 \leq \alpha \leq 0.1$). It is found in the $1/\nu$ regime that the inward shift of the plasma column, the negative pitch modulation and the $Bq = 100\%$ configuration are effective in reducing the diffusion coefficient (e.g., the diffusion coefficient for the configuration with $\Delta = -0.2$ m and $Bq = 100\%$ is about 1/10 that with $\Delta = 0$ m and $Bq = 0\%$.). This is caused by the side band structure of the magnetic field ripple (so-called multi-helicity effect). Comprehensive comparisons between the DKES code analysis and the multi-helicity theory developed by Shaing and Hokin have been made, and it is found that the theoretical correction due to the multi-helicity effect is in good agreement with the DKES calculations. In the ν regime, the DKES analysis shows that the diffusion coefficients are not as sensitive to the variation of the configuration. This characteristic supports the formula proposed by Crume et al., in which the diffusion coefficient is independent of the helical ripple in the ν regime. We have proposed a formula interpolating the diffusion coefficient between the $1/\nu$ and ν regimes, in which the correction due to the multi-helicity effect is incorporated.

As the ion temperature increases at a fixed density of $n = 10^{20}$ m^{-3}, the ion thermal transport transition from the $1/\nu$ regime to the ν regime occurs around $T_i = 2$-4 keV at $r/a \approx 0.5$, if a radial electric field $e\phi/T_i \approx 1$ is introduced. For an optimized configuration ($\Delta = -0.2$ m, $Bq = 100\%$), the ion thermal diffusivity has a maximum value of $\chi_i = 3.5$ m^2/s at around $T_i = 3$ keV with $e\phi/T_i \approx 1$, and the electron thermal diffusivity exceeds $\chi_e = 1.0$ m^2/s for $T_e > 3$ keV. The electron thermal diffusivity χ_e increases monotonically with T_e up to $T_e = 10$ keV.

The bootstrap current has been analyzed with the DKES code for the multi-helicity configurations of LHD. In the collisionless limit, the coefficient of the bootstrap current becomes independent of the collision frequency, and it is also insensitive to the radial electric field around $e\phi/T \approx 1$. These results support the assumptions employed in the theory to derive the formula for the bootstrap current in the banana regime. We have also confirmed that the analytic formula is applicable for various configurations of LHD. We should, however, remark that for collision frequencies between the plateau and the banana regimes, where the theory is not applicable, the bootstrap current might become larger than the collisionless limit by a factor of around two.

Acknowledgements

The authors wish to thank Dr. J. Todoroki for useful discussions.

references

[1] Miyamoto, K., Plasma Physics for Nuclear Fusion (MIT Press, Cambridge, 1976).

[2] Shaing, K.C., Phys. Fluids **27** (1984) 1567.

[3] Hastings, D.E., Houlberg, W.A., Shaing, K.C., Nucl. Fusion **25** (1985) 445.

[4] Potok, R.E., Politzer, P.A., Lidsky, L.M., Phys. Rev. Lett. **45** (1980) 1328.

[5] Boozer, A.H., Kuo-Petravic, G., Phys. Fluids **24** (1981) 851.

[6] Mynick, H.E., Phys. Fluids **25** (1982) 325.

[7] Lotz, W., Nuhrenberg, J., Phys. Fluids **31** (1988) 2984.

[8] Beidler, C.D., Hitchon, W.N.G., Grekov, D.L., Shishkin, A.A., Nucl. Fusion **30** (1990) 405.

[9] Hirshman, S.P., Shaing, K.C., van Rij W.I., Beasley, C.O., Crume, Jr., E.C., Phys. Fluids **29** (1986) 2951.

[10] van Rij, W.I., Hirshman, S.P., Phys. Fluids **B 1** (1989) 563.

[11] Crume Jr., E.C., Shaing, K.C., Hirshman, S.P., van Rij, W.I., Phys. Fluids **31** (1988) 11.

[12] Shaing, K.C., Crume Jr., E.C., Tolliver, J.S., Hirshman, S.P., van Rij, W.I., Phys. Fluids **B 1** (1989) 148.

[13] Renner, H., Gasparino, U., Maassberg, H., et al., in Plasma Physics and Controlled Nuclear Fusion Research, 1990, Washington, IAEA, IAEA-CN-53/C-1-2

[14] Yamada, H., Ida, K., Iguchi, H., Ogawa, Y., Howe, H.C., Bull. Am. Phys. Soc. **35** (1990) 2032.

[15] Murakami, M., Aceto, S.C., Anabitarte, E., et al., in Plasma Physics and Controlled Nuclear Fusion Research, 1990, Washington, IAEA, IAEA-CN-53/C-1-3

[16] Motojima, O., Akaishi, K., Asao, M., et al., in Plasma Physics and Controlled Nuclear Fusion Research, 1990, Washington, IAEA, IAEA-CN-53/G-1-5

[17] Sanuki, H., Todoroki, J. and Kamimura, T., Phys. Fluids **B 2** (1990) 2155.

[18] Nakajima, N., Okamoto, M., Todoroki, J., Nakamura, Y., Wakatani, M., Nucl. Fusion **29** (1989) 605.

[19] Yamazaki, K., Ohyabu, N., Okamoto, M., et al., in Plasma Physics and Controlled Nuclear Fusion Research, 1990, Washington, IAEA, IAEA-CN-53/C-4-11

[20] Mynick, H.E., Chu, T.K., Boozer, A.H., Phys. Rev. Lett. **48** (1982) 322.
[21] Shaing, K.C., Hokin, S.A., Phys. Fluids **26** (1983) 2136.
[22] Wagner, F., Becker, G., Behringer, K., et al., Phys. Rev. Lett. **49** (1982) 1408.
[23] Shaing, K.C., Callen, J.D., Phys. Fluids **26** (1983) 2315.
[24] Shaing, K.C., Hirshman, S.P., Tolliver, J.S., Phys. Fluids **29** (1986) 2548.
[25] Shaing, K.C., Hirshman, S.P., Callen, J.D., Phys. Fluids **29** (1986) 521.
[26] Shaing, K.C., Carreras, B.A., Dominguez, N., Lynch, V.E., Tolliver, J.S., Phys. Fluids **B 1** (1989) 1663.
[27] Murakami, M., Carreras, B.A., Baylor, L.R., et al., Phys. Rev. Lett. **66** (1991) 707.

Figure Captions

Fig. 1 D_{E1} calculated with DKES as a function of the mean free path (denoted $CMUL = \nu/v$: m^{-1}), where the radial electric field is introduced with the parameter $EFIELD$ (= E_r/v : $V \cdot s/m^2$). To calculate the thermal diffusivity $\chi_{i,e}$,these data must be integrated along a path shown by a broken line with a weight of a Maxwellian distribution function.

Fig. 2 D_{E1} values as functions of (a) toroidal ripple and (b) helical ripple, where a model field defined by $B/B_0 = 1 - \varepsilon_t\cos(\theta) + \varepsilon_h\cos(l\theta - m\phi)$ with l=2 and m=10 is employed. Scalings represented by eqs. (2), (3a) and (3b) are also plotted. $EFIELD$ values are (i) 10^{-6}, (ii) 10^{-4}, (iii) $3x10^{-4}$, (iv) 10^{-3}, (v) $3x10^{-3}$ and (vi) 10^{-2}.

Fig. 3 D_{E1} values as a function of the radial electric field for single- and multi-helicity cases, where two different configurations (case(a): Δ = -0.2 m, Bq = 100%, and case (b): Δ = 0 m, Bq = 0%) are dealt with. Toroidal/helical ripples are listed in Table II, including the correction factor due to the multi-helicity effect.

Fig. 4 Fourier components of the magnetic field (case (a): Δ = -0.2 m, Bq = 100%, and case (b): Δ = 0 m, Bq = 0%). The magnetic field ripple along the field line at $r/a \approx 0.5$ (shown with arrows) is also plotted. Poloidal and toroidal Fourier mode numbers are denoted by l and m, respectively.

Fig. 5 D_{E1} values as a function of the plasma minor radius for various positions of the plasma column (Δ = 0, -0.1, -0.2 m) in the $1/\nu$ ($EFIELD$=10^{-6}) and ν ($EFIELD$=10^{-2}) regimes. The corresponding structure of the magnetic field ripple is also presented.

Fig. 6 D_{E1} values as a function of the plasma minor radius for various quadrupole fields (Bq = 0%, 100%, 200%) in the $1/\nu$ and ν regimes. The configuration with Bq = 100% corresponds to a toroidally averaged plasma shape with a circular cross section. The corresponding structure of the magnetic field ripple is also presented.

Fig. 7 D_{E1} values as a function of the plasma minor radius for various pitch modulations of the helical coil (α = -0.1, 0, 0.1) at the $1/\nu$ and ν regimes. The corresponding structure of the magnetic field ripple is also presented.

Fig. 8 Comparison of the DKES data with the scaling of the helical ripple in the $1/\nu$ regime. DKES data are plotted as functions of (a) $\Lambda_s = \varepsilon_t^2\varepsilon_h^{3/2}/B_0^2$ and (b) $\Lambda_m = C_m\varepsilon_t^2\varepsilon_h^{3/2}/B_0^2$, where C_m is a correction factor due to the multi-helicity effect, originated by the theory of Shaing and Hokin.

Fig. 9 Interpolation formula between $1/\nu$ and ν regimes, corrected for the multi-helicity effect. Open and closed circles denote the DKES calculation results for single and multi-helicity, respectively. Using a correction factor C_m due to the multi-helicity effect, defined by eq. (5), the diffusion coefficients D_m for the multi-helicity case are calculated as $D_m = D_s(R_c + 1)/(R_c + 1/C_m)$ with the single-helicity data D_s shown by dotted line, where R_c is the ratio of the diffusion coefficients of the ν regime to those of the $1/\nu$ regime.

Fig.10 The ion thermal diffusivity χ_i as a function of the collision frequency for case (a): Δ = -0.2 m, Bq = 100%, and case (b): Δ = 0 m, Bq = 0%, where the ion temperature is changed at a fixed density of $n = 10^{20}\mathrm{m}^{-3}$. The radial electric field E_r is converted into a potential defined by $E_r = -e \text{ grad } \phi = -e\phi/a_\phi$ with a_ϕ = 0.6 m, and the value of $e\phi/T_{i,e}$ is fixed for each curve. With no radial electric field in the $1/\nu$ regime, the ion thermal diffusivity χ_i is proportional to $T_i^{7/2}$

Fig.11 The electron thermal diffusivity χ_e for case (a): Δ = -0.2 m, Bq = 100%, and case (b): Δ = 0 m, Bq = 0%, where the electron temperature is changed at a fixed density of $n = 10^{20}\mathrm{m}^{-3}$.

Fig.12 Peak values of χ_i presented in Fig. 10 for various densities as a function of an ion temperature which gives the peak in the χ_i value at $e\phi/T_i$=1. The range of the ion temperature with $\chi_i > 0.9\chi_i(peak)$ is also presented. Arrows indicate the ion temperature with $\chi_i(peak)$, calculated by eq. (9).

Fig.13 D_{E3} values from DKES as a function of the collision frequency ($CMUL$) for various radial electric fields $e\phi/T_i$,. Values for an equivalent tokamak are also shown: they are obtained by setting all helical ripples to be zero in the DKES code.

Fig.14 D_{E1} and D_{E3} values as a function of the radial electric field.

Fig.15 D_{E3} values as a function of the radial electric field for different plasma minor radii (i.e., for different magnetic field ripples) in the configuration of case (a) (Δ = -0.2 m, Bq = 100%).

Fig.16 The bootstrap current normalized by that of the equivalent tokamak as a function of the minor radius, where the plateau values in Fig. 15 are included. Theoretical values are calculated with eq. (10). Single- and multi-helicity configurations are compared for two cases.

Fig.17 D_{E3} values as a function of the quadrupole field component Bq. The toroidally averaged plasma shapes are schematically drawn for each Bq value, and the configuration with Bq = 100% is corresponding to a toroidally averaged plasma shape with a circular cross section.

Table Captions

Table I Specifications of the Large Helical Device (LHD). A few parameters employed in transport analysis are slightly different with these specified values. Values in brackets are used in the DKES code.

Major radius	R = 3.9 m (4.0 m)
Minor radius	a = 0.5 - 0.65 m
Toroidal field	$B_0 = 4$ T
Helical coils	
pitch number	$m = 10$
pitch parameter $\gamma=(m/l)(a_c/R_c)$	$\gamma = 1.25$ (1.2)
pitch modulation	$\alpha = 0.1$
maximum field	$B_{max} = 9.6$ T

Table II Magnetic field ripples for two configurations.

	case (a) (Δ = -0.2 m, Bq = 100%)	case (b) (Δ = 0 m, Bq = 0%)
ε_t	5.84 %	6.21 %
ε_h	4.78 %	4.83 %
$\varepsilon_t^2\varepsilon_h^{3/2}$	$3.56\mathrm{x}10^{-5}$	$4.09\mathrm{x}10^{-5}$
$C_m(=F_m/F_s)$	0.55	2.75
$C_m\varepsilon_t^2\varepsilon_h^{3/2}$	$1.96\mathrm{x}10^{-5}$	$11.2\mathrm{x}10^{-5}$

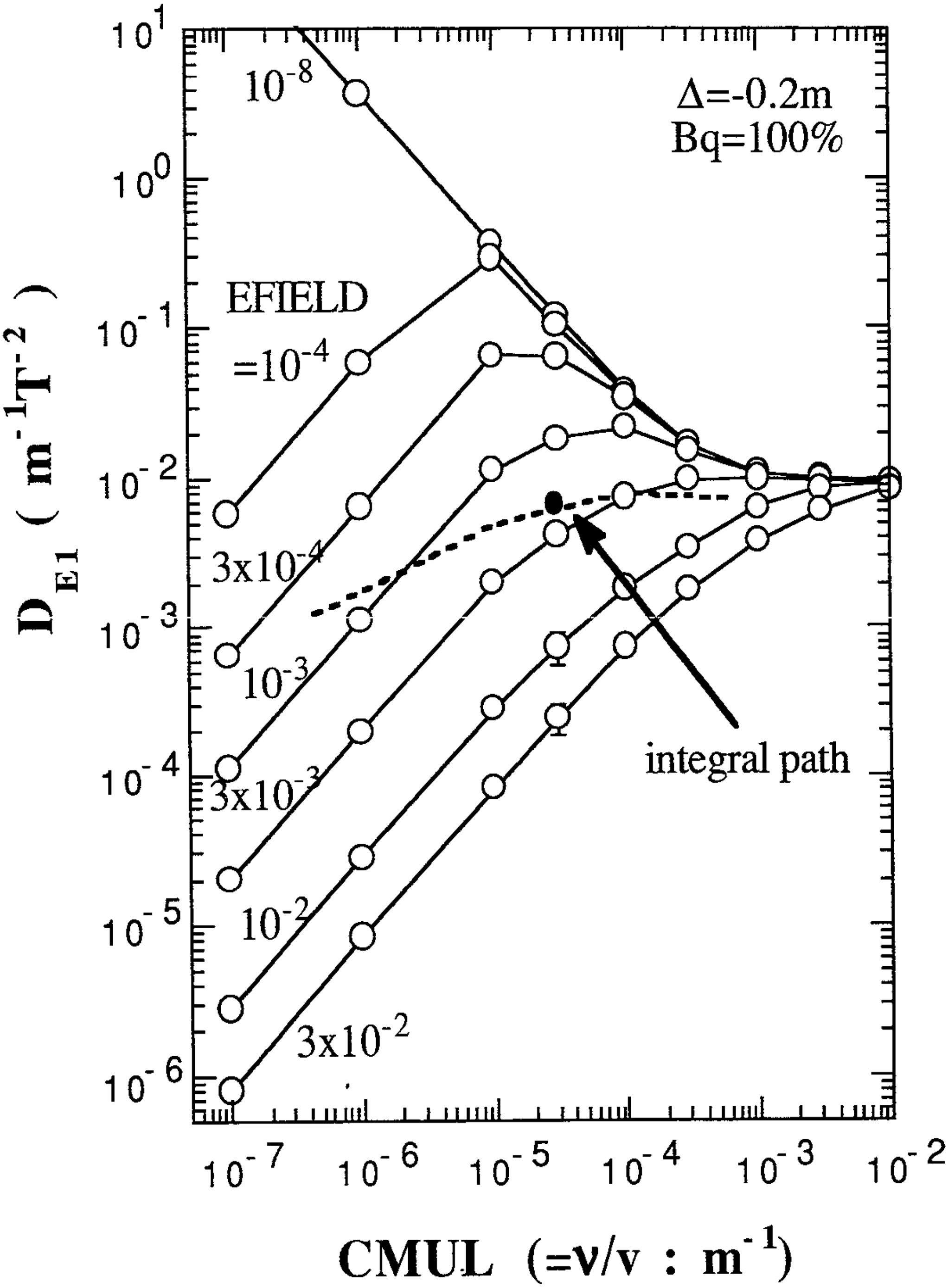

10-8
Δ=-0.2m
Bq=100%
EFIELD
=10-4
3x10-4
10-3
3x10-3
10-2
3x10-2
integral path
D_E1 (m-1T-2)
CMUL (=ν/v : m-1)
10 1
10 0
10-1
10-2
10-3
10-4
10-5
10-6
10-7
10-6
10-5
10-4
10-3
10-2

Fig. 1

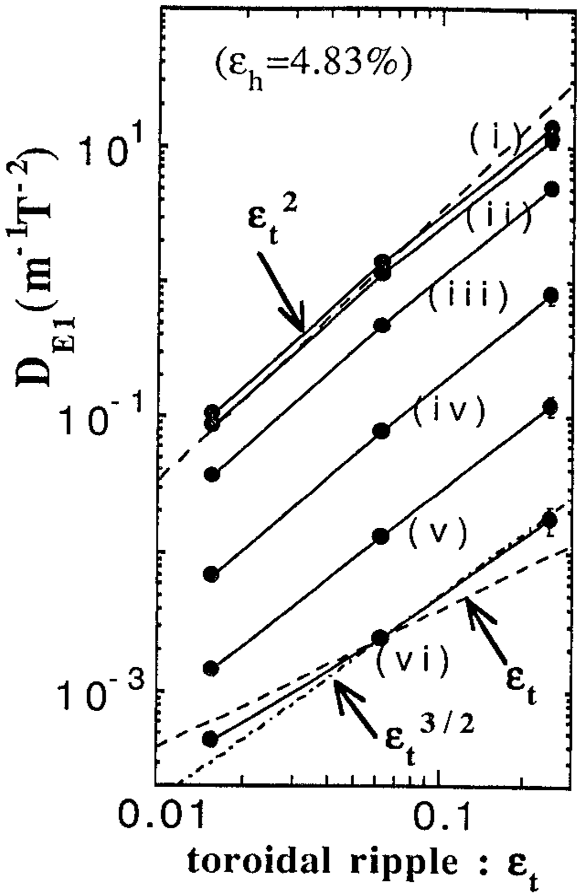

(ε_h=4.83%)
$D_{E1}(m^{-1}T^{-2})$
10^{1}
10^{-1}
10^{-3}
0.01
0.1
toroidal ripple : ε_t
$\varepsilon_t^{\ 2}$
ε_t
$\varepsilon_t^{\ 3/2}$
(i)
(ii)
(iii)
(iv)
(v)
(vi)

Fig. 2(a)

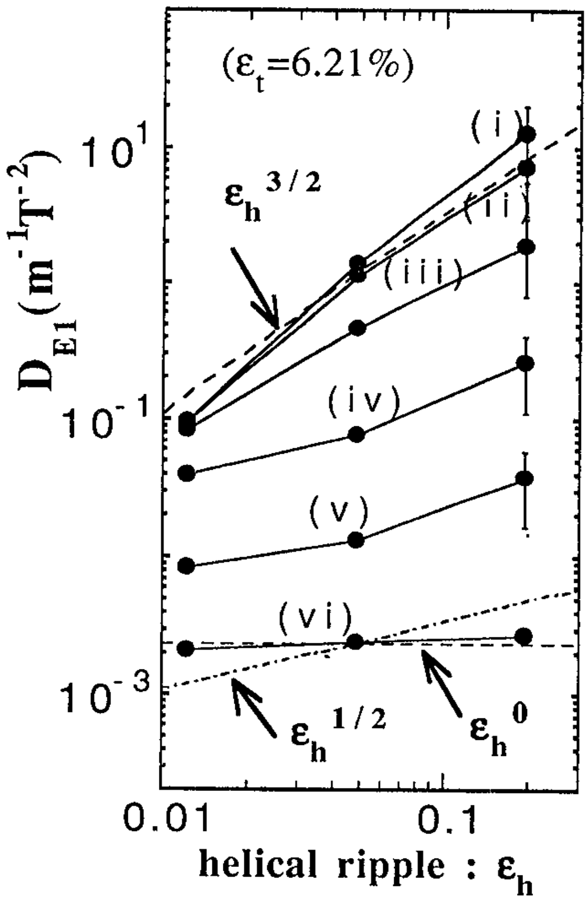

(ε_t=6.21%)
$D_{E1}(m^{-1}T^{-2})$
10^{1}
10^{-1}
10^{-3}
0.01
0.1
helical ripple : ε_h
$\varepsilon_h^{\ 3/2}$
$\varepsilon_h^{\ 1/2}$
$\varepsilon_h^{\ 0}$
(i)
(ii)
(iii)
(iv)
(v)
(vi)

Fig. 2(b)

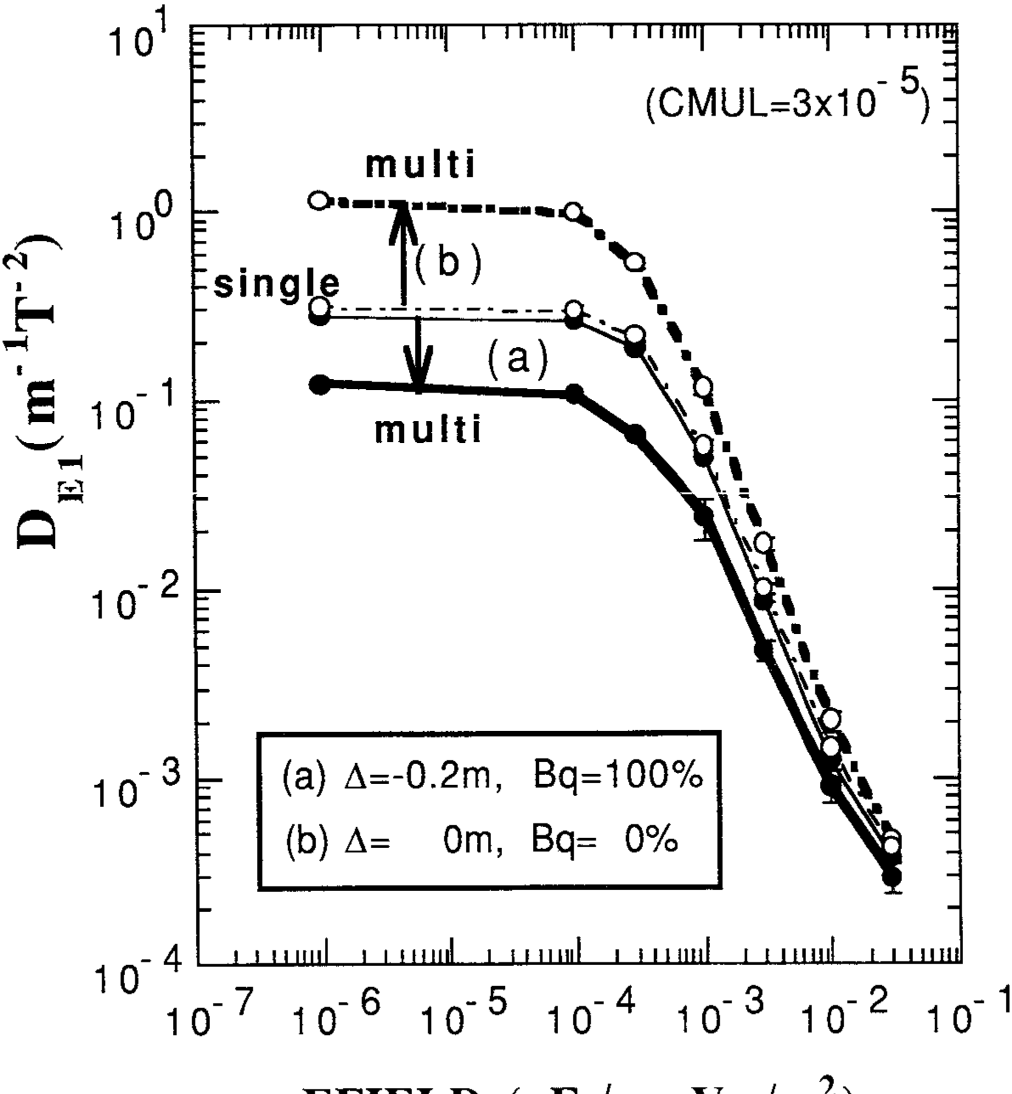

(CMUL=3x10^{-5})
multi
single
(b)
(a)
multi
(a) Δ=-0.2m, Bq=100%
(b) Δ= 0m, Bq= 0%
D_{E1} ($m^{-1}T^{-2}$)
EFIELD (=E_r/v : V·s/m^2)
10^{1}
10^{0}
10^{-1}
10^{-2}
10^{-3}
10^{-4}
10^{-7}
10^{-6}
10^{-5}
10^{-4}
10^{-3}
10^{-2}
10^{-1}

Fig. 3

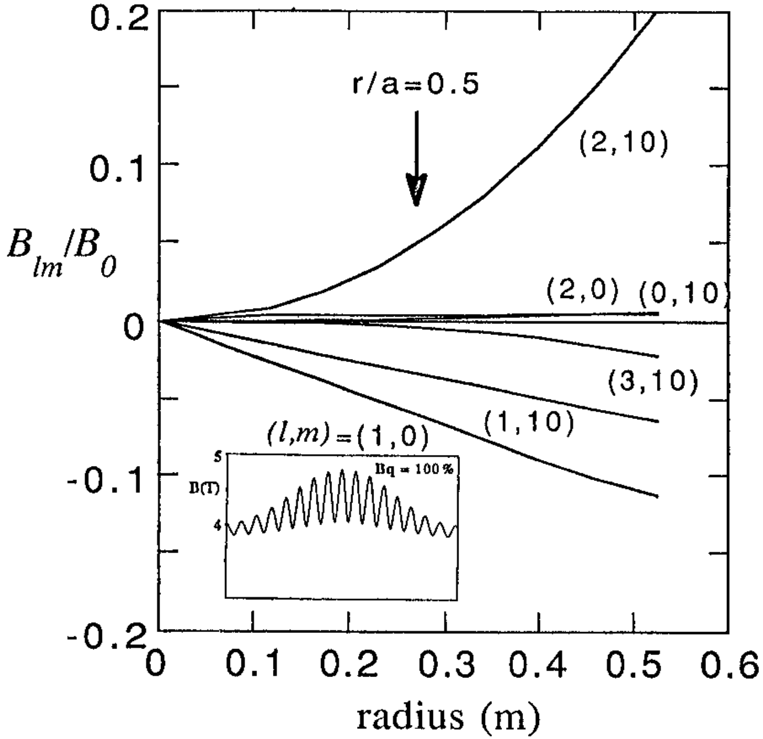

0.2
0.1
0
-0.1
-0.2
B_{lm}/B_0
r/a=0.5
(2,10)
(2,0)
(0,10)
(3,10)
(1,10)
(l,m)=(1,0)
5
B(T)
4
Bq = 100 %
0
0.1
0.2
0.3
0.4
0.5
0.6
radius (m)

Fig. 4(a)

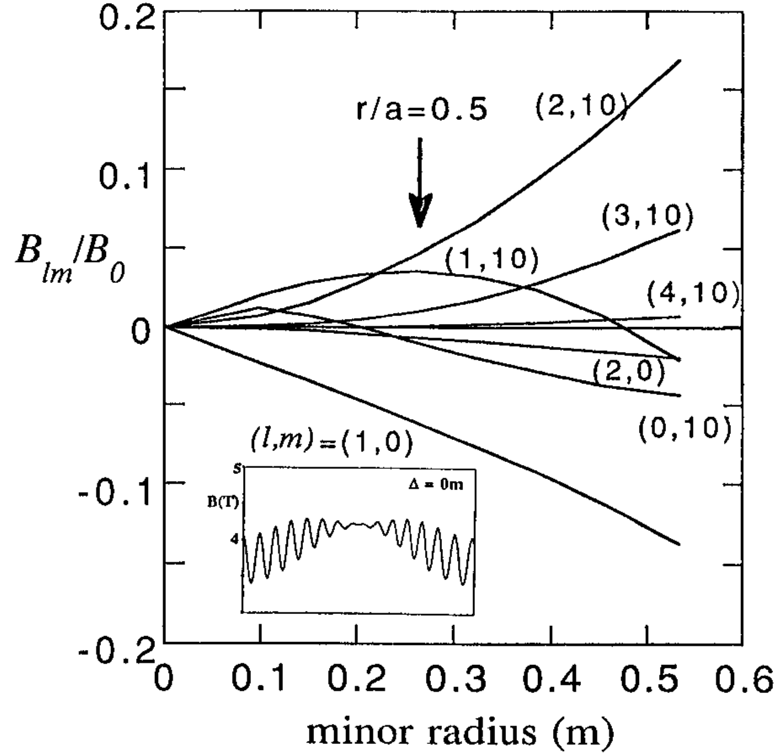

0.2
0.1
0
-0.1
-0.2
B_{lm}/B_0
r/a=0.5
(2,10)
(3,10)
(1,10)
(4,10)
(2,0)
(0,10)
(l,m)=(1,0)
5
B(T)
4
Δ = 0m
0
0.1
0.2
0.3
0.4
0.5
0.6
minor radius (m)

Fig. 4(b)

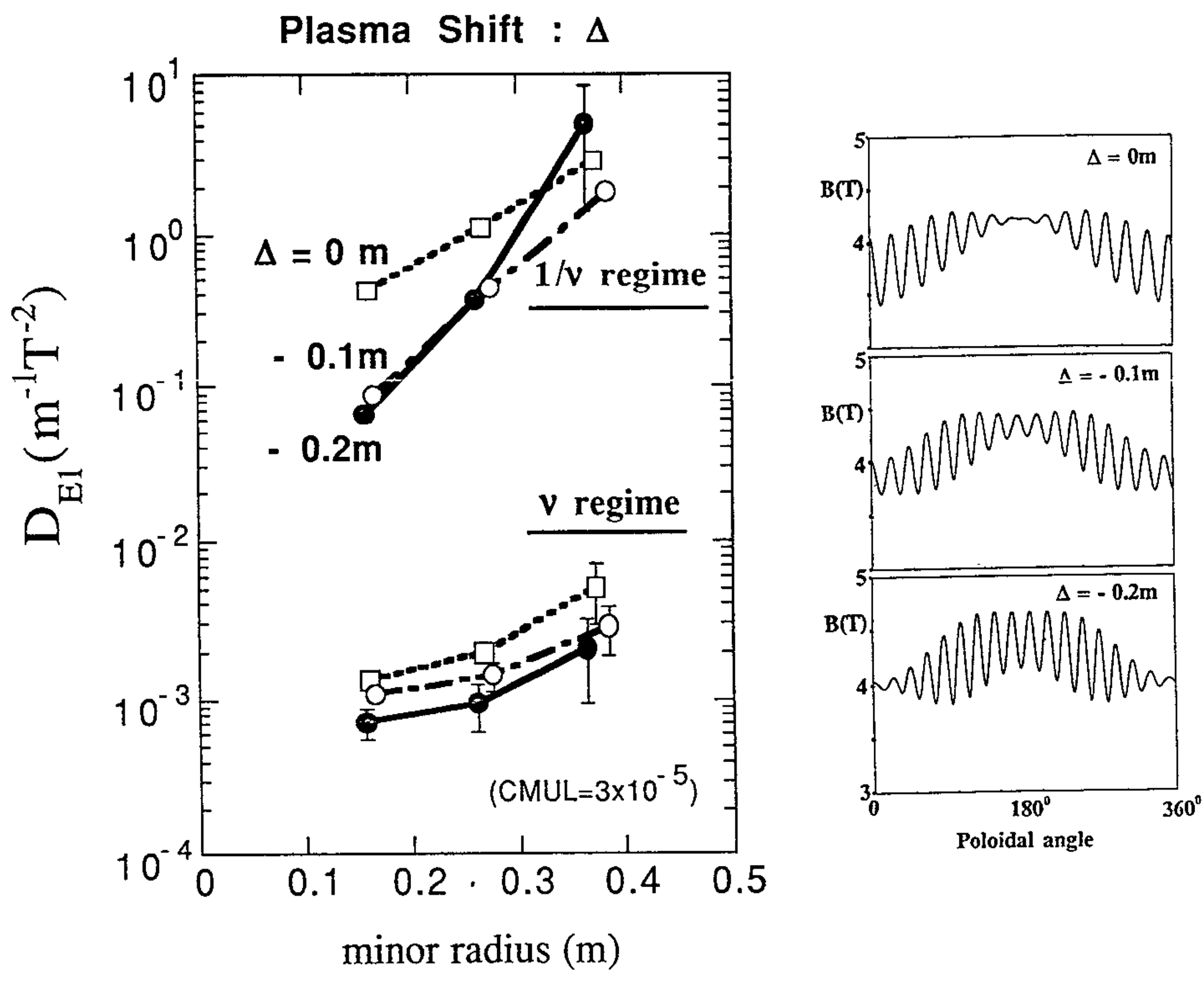
Plasma Shift : Δ
$D_{E1}(m^{-1}T^{-2})$
Δ = 0 m
- 0.1m
- 0.2m
1/ν regime
ν regime
(CMUL=3x10^{-5})
minor radius (m)
Δ = 0m
Δ = - 0.1m
Δ = - 0.2m
B(T)
Poloidal angle

Fig. 5

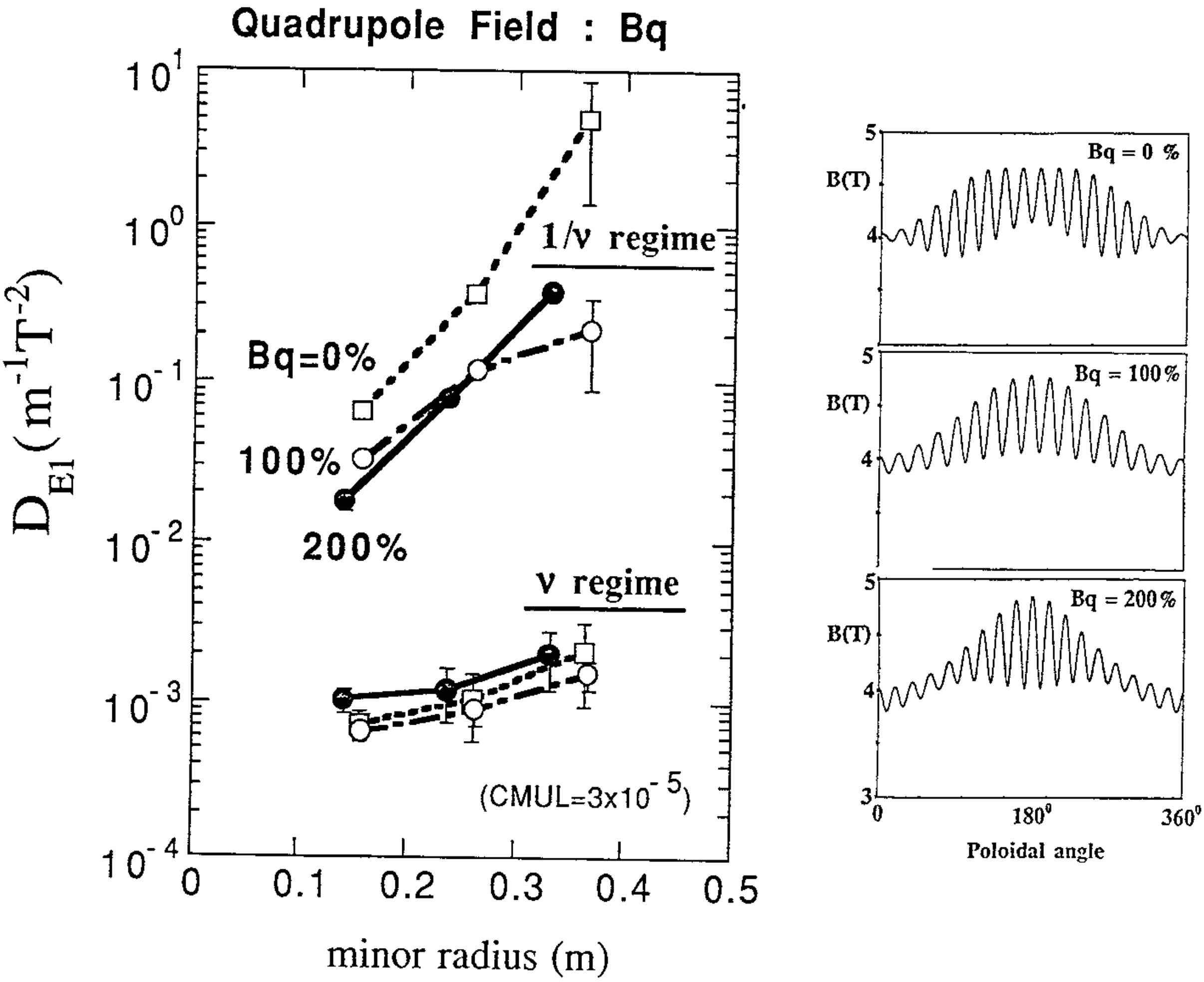

Quadrupole Field : Bq
$D_{E1}(m^{-1}T^{-2})$
1/ν regime
Bq=0%
100%
200%
ν regime
(CMUL=3x10^-5)
minor radius (m)
Bq = 0 %
Bq = 100 %
Bq = 200 %
B(T)
Poloidal angle

Fig. 6

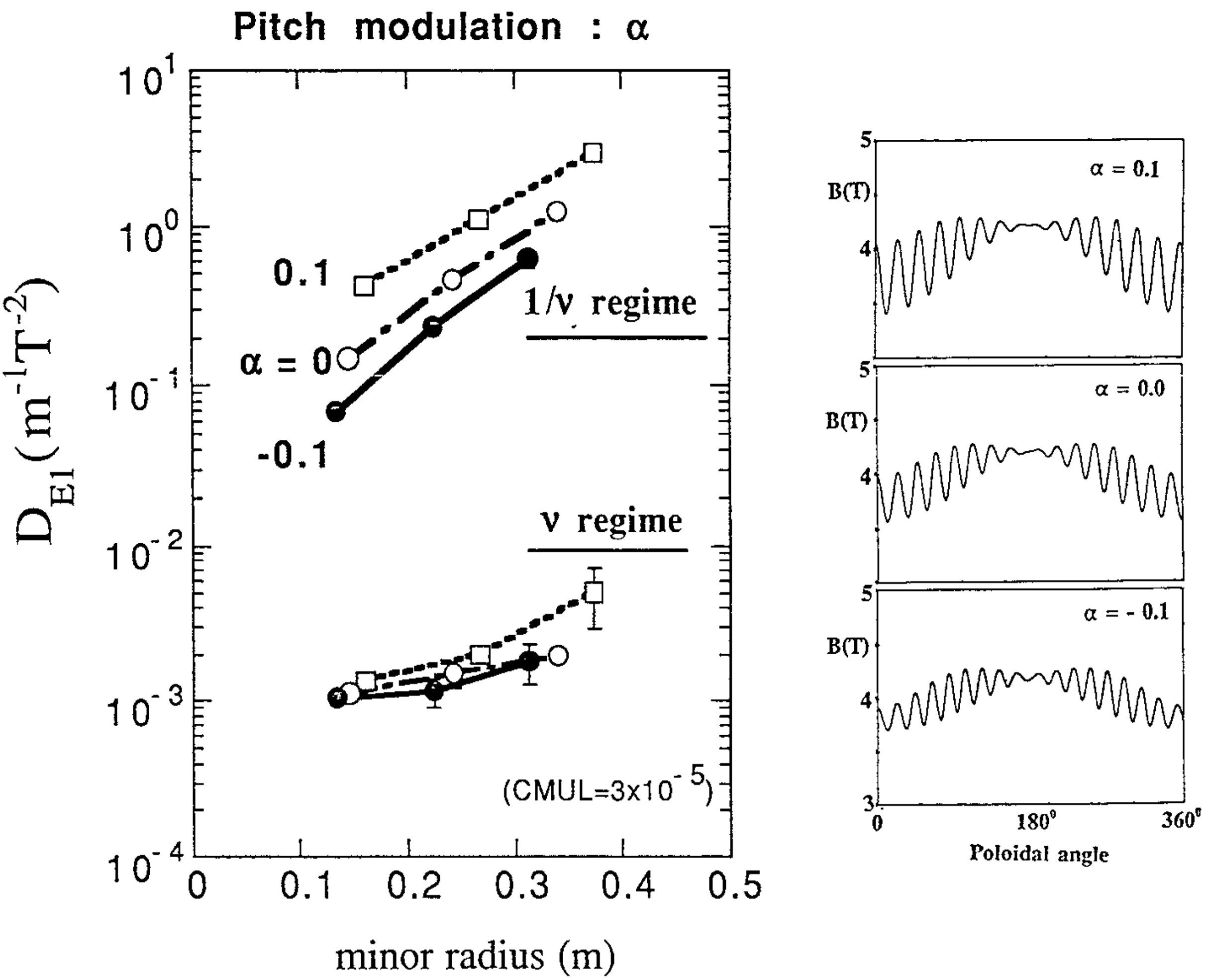
Pitch modulation : α
$D_{E1}(m^{-1}T^{-2})$
minor radius (m)
0.1
α = 0
-0.1
1/ν regime
ν regime
(CMUL=3x10^{-5})
10^{1}
10^{0}
10^{-1}
10^{-2}
10^{-3}
10^{-4}
0
0.1
0.2
0.3
0.4
0.5
α = 0.1
α = 0.0
α = - 0.1
B(T)
5
4
3
0
180°
360°
Poloidal angle

Fig. 7

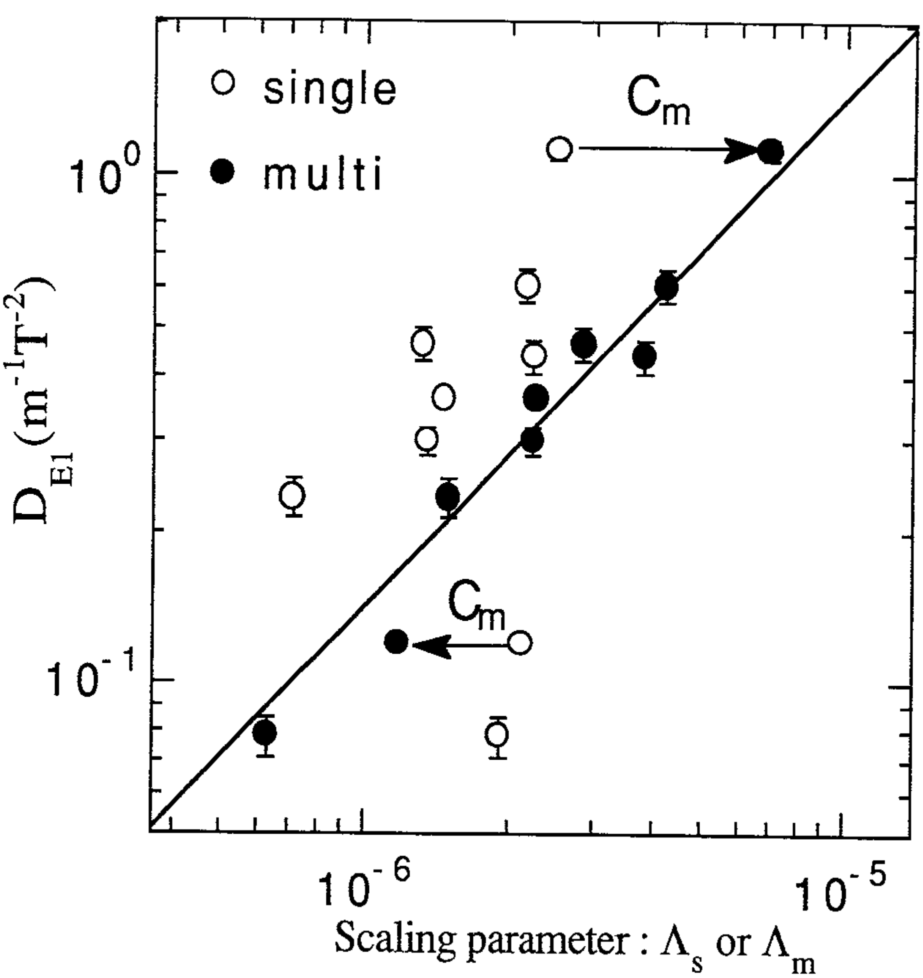

single
multi
Cm
Cm
10^0
10^{-1}
D_{E1} ($m^{-1}T^{-2}$)
10^{-6}
10^{-5}
Scaling parameter : Λ_s or Λ_m

Fig. 8

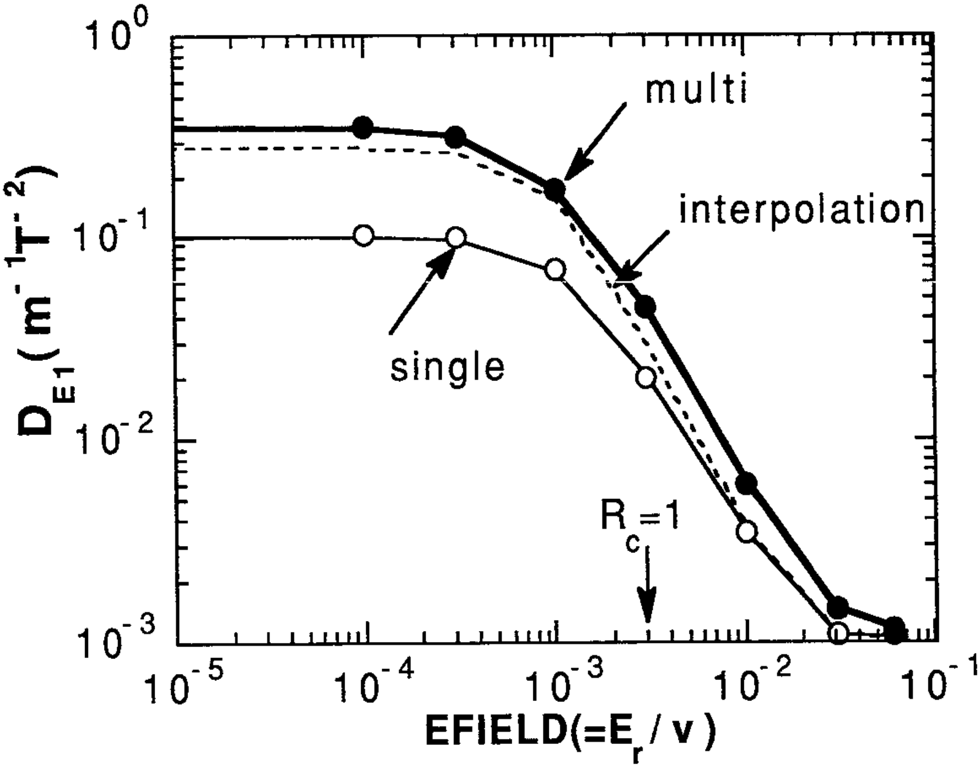

multi
interpolation
single
$R_c=1$
10^0
10^{-1}
10^{-2}
10^{-3}
$D_{E1}(m^{-1}T^{-2})$
10^{-5}
10^{-4}
10^{-3}
10^{-2}
10^{-1}
EFIELD($=E_r/v$)

Fig. 9

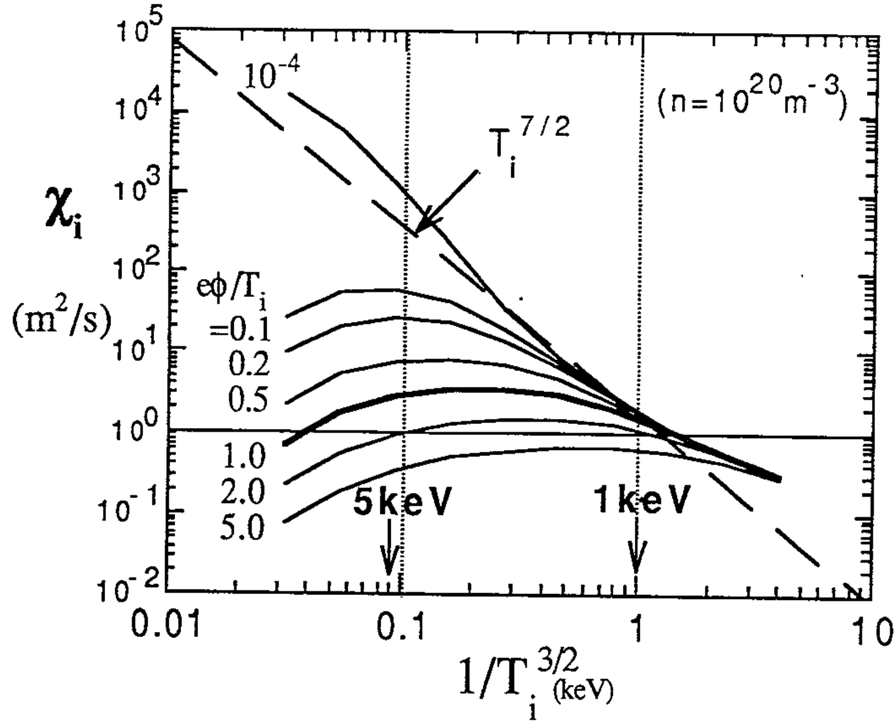

Fig. 10(a)

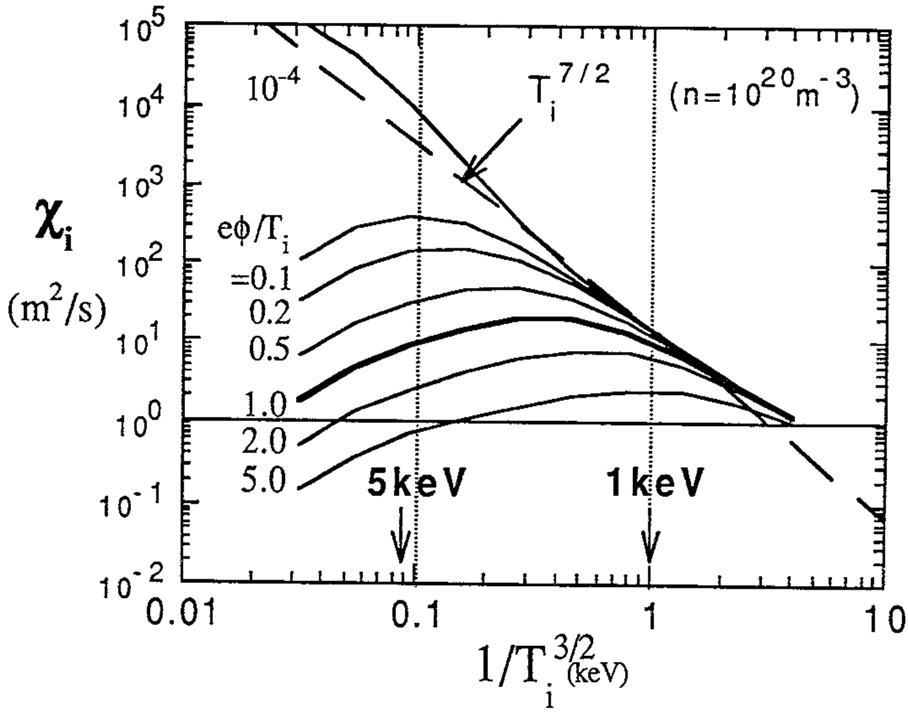

Fig. 10(b)

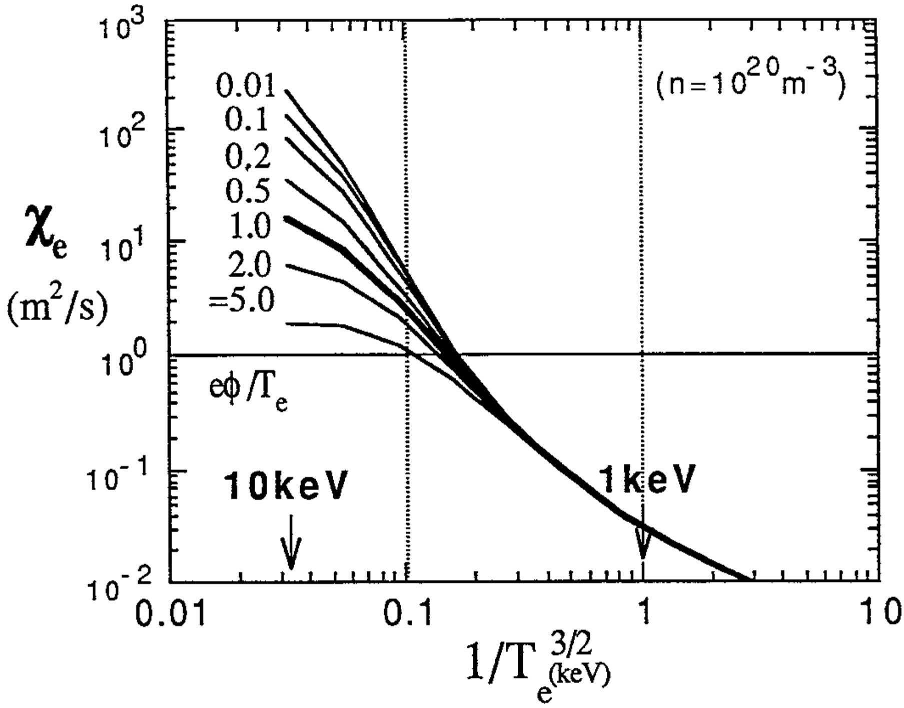

Fig. 11(a)

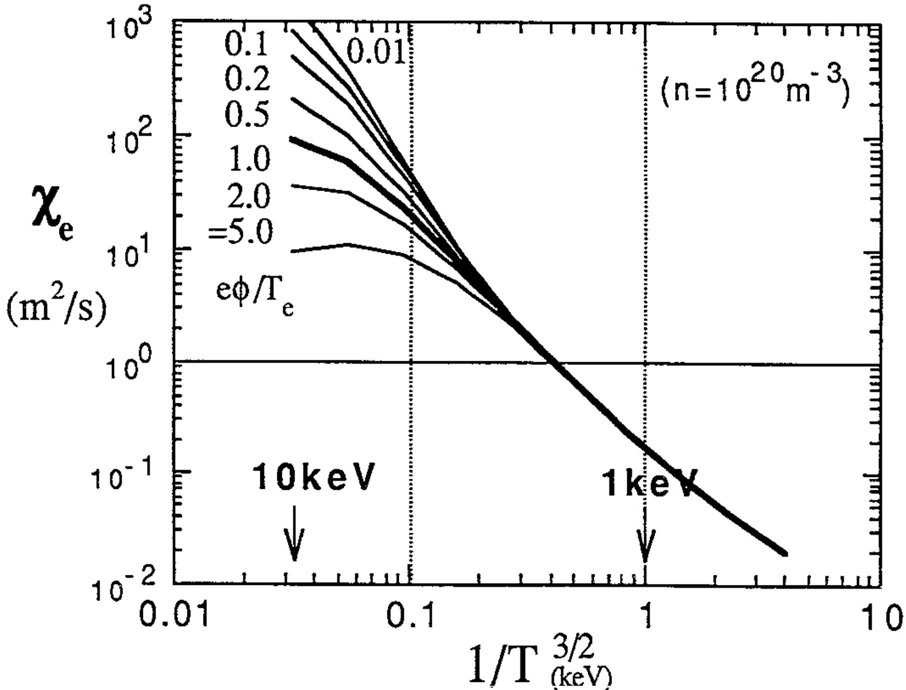

Fig. 11(b)

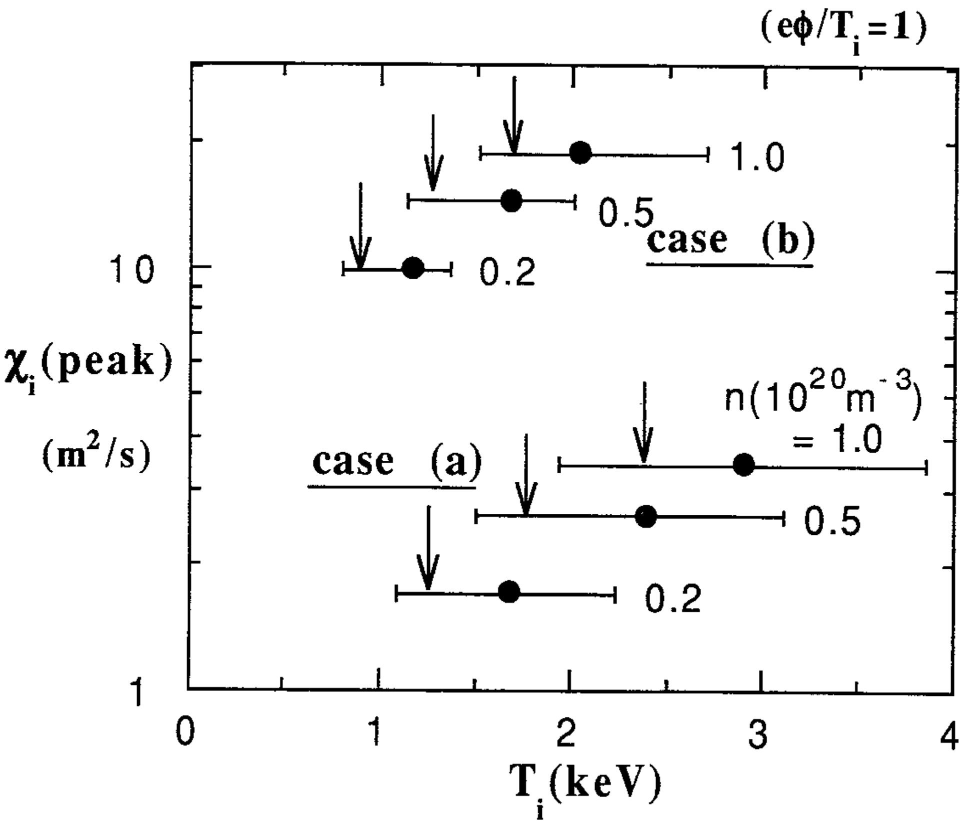

$(e\phi/T_i = 1)$
1.0
0.5
case (b)
10
0.2
χ_i(peak)
(m^2/s)
$n(10^{20}m^{-3})$
= 1.0
case (a)
0.5
0.2
1
0
1
2
3
4
T_i(keV)

Fig. 12

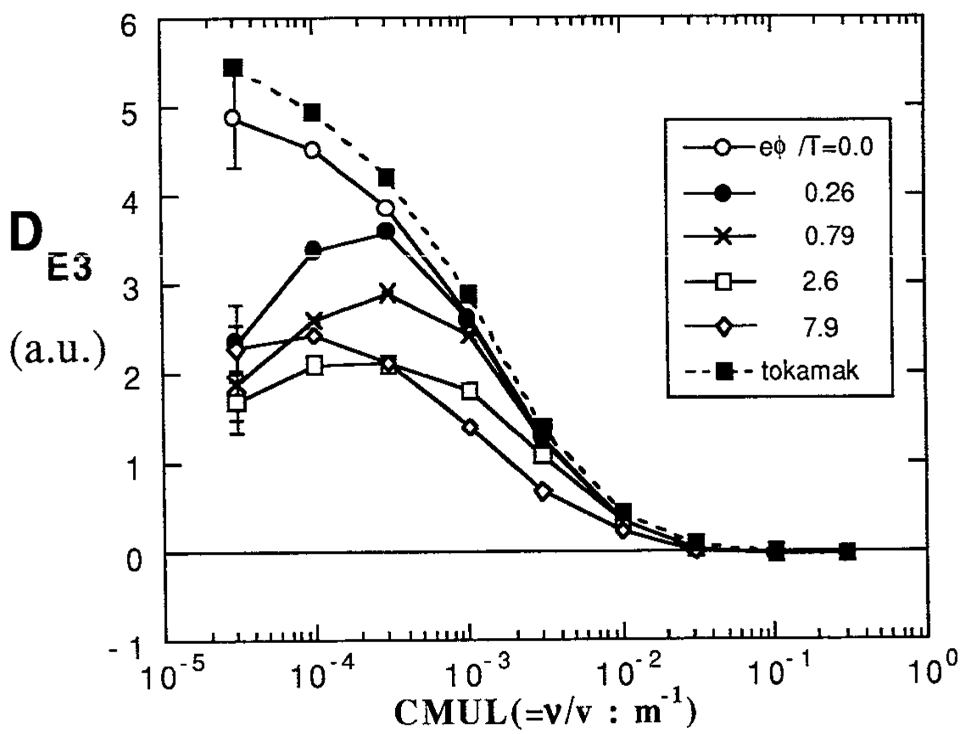
6
5
4
3
2
1
0
- 1
D E3
(a.u.)
10^-5
10^-4
10^-3
10^-2
10^-1
10^0
CMUL(=ν/v : m^-1)
eφ /T=0.0
0.26
0.79
2.6
7.9
tokamak

Fig. 13

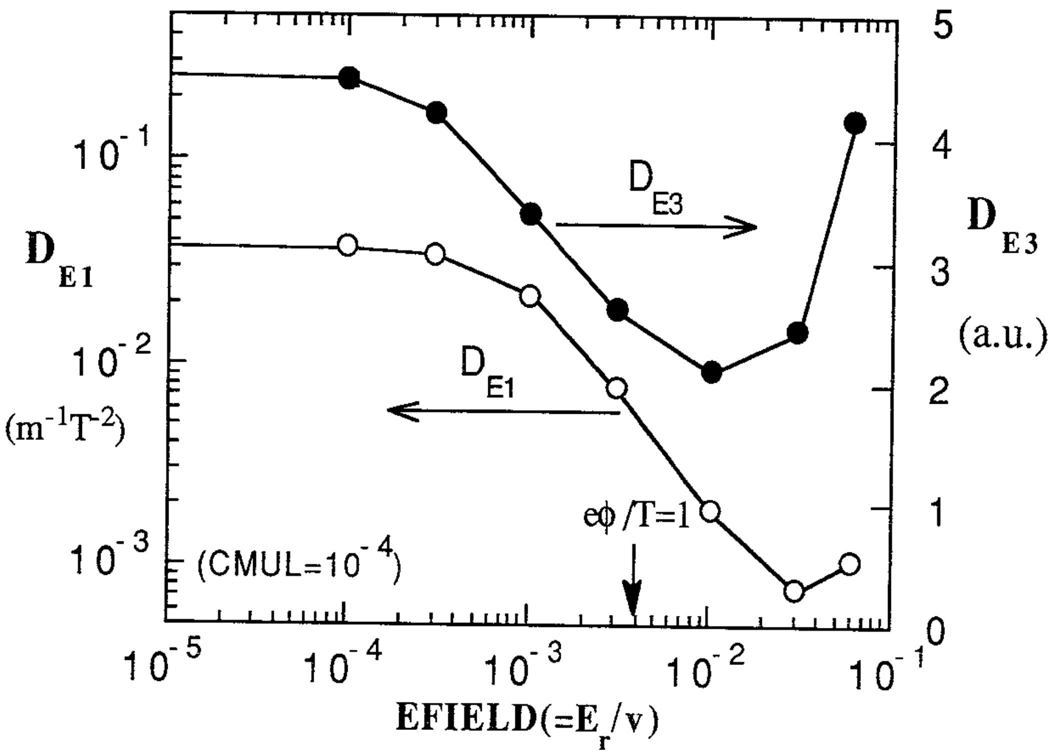

10^-1
10^-2
10^-3
D E1
(m^-1T^-2)
(CMUL=10^-4)
D E3
D E1
eφ/T=1
5
4
3
2
1
0
D E3
(a.u.)
10^-5
10^-4
10^-3
10^-2
10^-1
EFIELD(=E_r/v)

Fig. 14

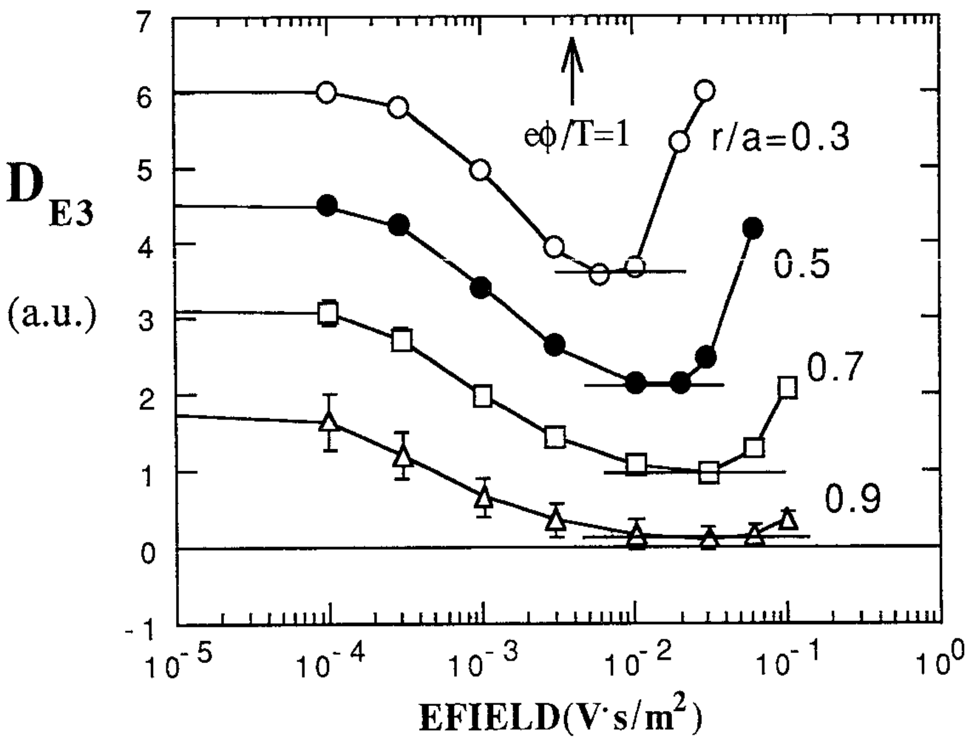

D_E3
(a.u.)
eϕ/T=1
r/a=0.3
0.5
0.7
0.9
7
6
5
4
3
2
1
0
-1
10^-5
10^-4
10^-3
10^-2
10^-1
10^0
EFIELD(V·s/m^2)

Fig. 15

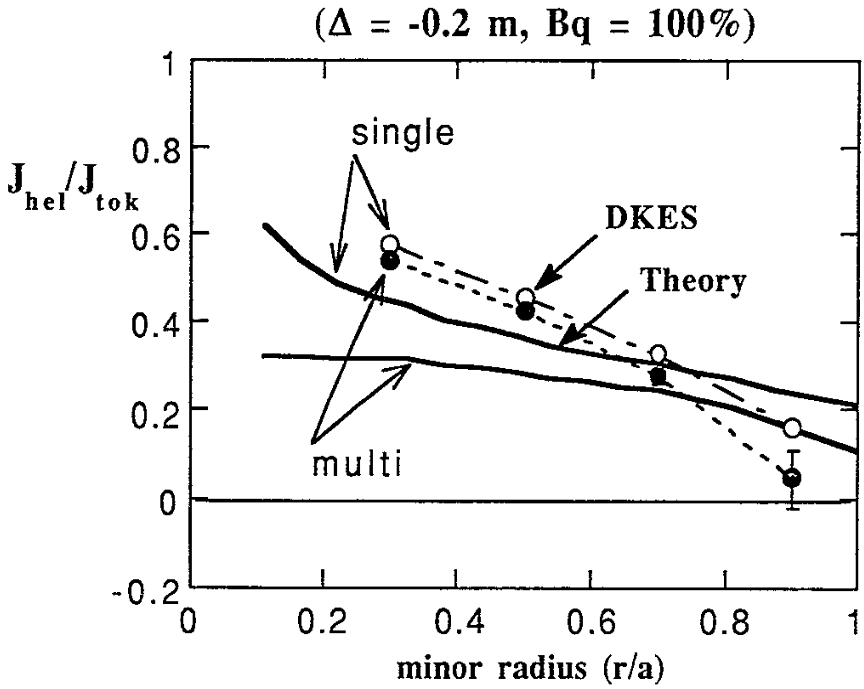

Fig. 16(a)

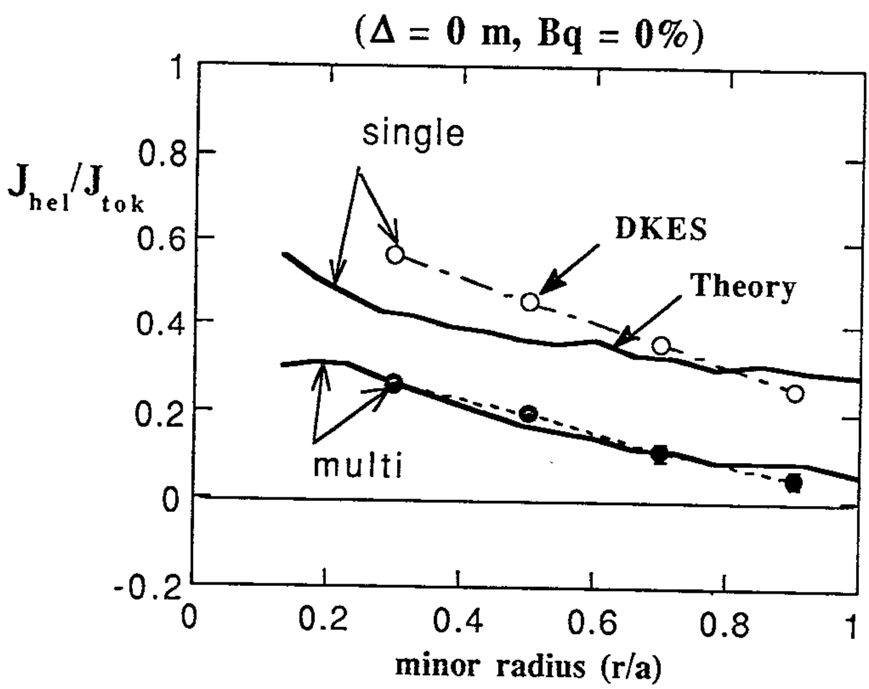

Fig. 16(b)

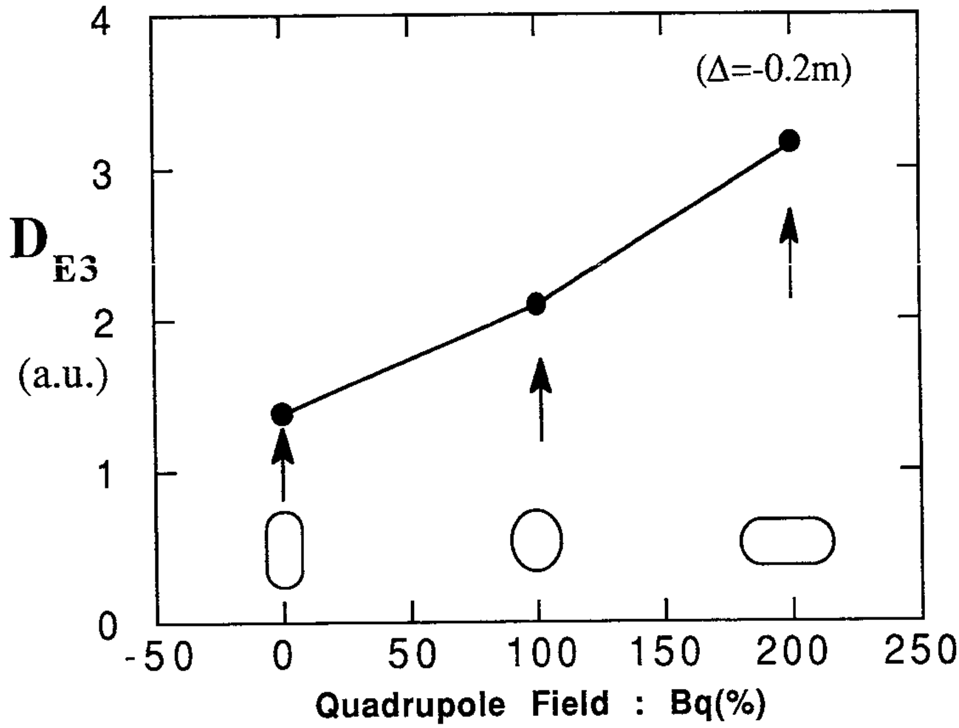

Fig. 17

Recent Issues of NIFS Series

NIFS-50 S.Koide, *3-Dimensional Simulation of Dynamo Effect of Reversed Field Pinch*; Sep. 1990

NIFS-51 O.Motojima, K. Akaishi, M.Asao, K.Fujii, J.Fujita, T.Hino, Y.Hamada, H.Kaneko, S.Kitagawa, Y.Kubota, T.Kuroda, T.Mito, S.Morimoto, N.Noda, Y.Ogawa, I.Ohtake, N.Ohyabu, A.Sagara, T. Satow, K.Takahata, M.Takeo, S.Tanahashi, T.Tsuzuki, S.Yamada, J.Yamamoto, K.Yamazaki, N.Yanagi, H.Yonezu, M.Fujiwara, A.Iiyoshi and LHD Design Group, *Engineering Design Study of Superconducting Large Helical Device*; Sep. 1990

NIFS-52 T.Sato, R.Horiuchi, K. Watanabe, T. Hayashi and K.Kusano, *Self-Organizing Magnetohydrodynamic Plasma*; Sep. 1990

NIFS-53 M.Okamoto and N.Nakajima, *Bootstrap Currents in Stellarators and Tokamaks*; Sep. 1990

NIFS-54 K.Itoh and S.-I.Itoh, *Peaked-Density Profile Mode and Improved Confinement in Helical Systems*; Oct. 1990

NIFS-55 Y.Ueda, T.Enomoto and H.B.Stewart, *Chaotic Transients and Fractal Structures Governing Coupled Swing Dynamics*; Oct. 1990

NIFS-56 H.B.Stewart and Y.Ueda, *Catastrophes with Indeterminate Outcome*; Oct. 1990

NIFS-57 S.-I.Itoh, H.Maeda and Y.Miura, *Improved Modes and the Evaluation of Confinement Improvement*; Oct. 1990

NIFS-58 H.Maeda and S.-I.Itoh, *The Significance of Medium- or Small-size Devices in Fusion Research*; Oct. 1990

NIFS-59 A.Fukuyama, S.-I.Itoh, K.Itoh, K.Hamamatsu, V.S.Chan, S.C.Chiu, R.L.Miller and T.Ohkawa, *Nonresonant Current Drive by RF Helicity Injection*; Oct. 1990

NIFS-60 K.Ida, H.Yamada, H.Iguchi, S.Hidekuma, H.Sanuki, K.Yamazaki and CHS Group, *Electric Field Profile of CHS Heliotron/Torsatron Plasma with Tangential Neutral Beam Injection*; Oct. 1990

NIFS-61 T.Yabe and H.Hoshino, *Two- and Three-Dimensional Behavior of Rayleigh-Taylor and Kelvin-Helmholz Instabilities*; Oct. 1990

NIFS-62 H.B. Stewart, *Application of Fixed Point Theory to Chaotic Attractors of Forced Oscillators;* Nov. 1990

NIFS-63 K.Konn., M.Mituhashi, Yoshi H.Ichikawa,*Soliton on Thin Vortex Filament;* Dec. 1990

NIFS-64 K.Itoh, S.-I.Itoh and A.Fukuyama,*Impact of Improved Confinement on Fusion Research;* Dec. 1990

NIFS -65 A.Fukuyama, S.-I.Itoh and K. Itoh,*A Consistency Analysis on the Tokamak Reactor Plasmas;* Dec. 1990

NIFS-66 K.Itoh, H. Sanuki, S.-I. Itoh and K. Tani,*Effect of Radial Electric Field on α-Particle Loss in Tokamaks;* Dec. 1990

NIFS-67 K.Sato,and F.Miyawaki,*Effects of a Nonuniform Open Magnetic Field on the Plasma Presheath*; Jan.1991

NIFS-68 K.Itoh and S.-I.Itoh,*On Relation between Local Transport Coefficient and Global Confinement Scaling Law;* Jan. 1991

NIFS-69 T.Kato, K.Masai, T.Fujimoto,F.Koike, E.Källne, E.S.Marmar and J.E.Rice,*He-like Spectra Through Charge Exchange Processes in Tokamak Plasmas;* Jan.1991

NIFS-70 K. Ida, H. Yamada, H. Iguchi, K. Itoh and CHS Group, *Observation of Parallel Viscosity in the CHS Heliotron/Torsatron* ; Jan.1991

NIFS-71 H. Kaneko, *Spectral Analysis of the Heliotron Field with the Toroidal Harmonic Function in a Study of the Structure of Built-in Divertor* ; Jan. 1991

NIFS-72 S. -I. Itoh, H. Sanuki and K. Itoh, *Effect of Electric Field Inhomogeneities on Drift Wave Instabilities and Anomalous Transport* ; Jan. 1991

NIFS-73 Y.Nomura, Yoshi.H.Ichikawa and W.Horton, *Stabilities of Regular Motion in the Relativistic Standard Map*; Feb. 1991

NIFS-74 T.Yamagishi, *Electrostatic Drift Mode in Toroidal Plasma with Minority Energetic Particles,* Feb. 1991

NIFS-75 T.Yamagishi, *Effect of Energetic Particle Distribution on Bounce Resonance Excitation of the Ideal Ballooning Mode*, Feb. 1991

NIFS-76 T.Hayashi, A.Tadei, N.Ohyabu and T.Sato, *Suppression of Magnetic Surface Breading by Simple Extra Coils in Finite Beta Equilibrium of Helical System;* Feb. 1991

NIFS-77 N. Ohyabu, *High Temperature Divertor Plasma Operation*; Feb. 1991

NIFS-78 K.Kusano, T. Tamano and T. Sato, *Simulation Study of Toroidal Phase-Locking Mechanism in Reversed-Field Pinch Plasma*; Feb. 1991

NIFS-79 K. Nagasaki, K. Itoh and S. -I. Itoh, *Model of Divertor Biasing and Control of Scrape-off Layer and Divertor Plasmas*; Feb. 1991

NIFS-80 K. Nagasaki and K. Itoh, *Decay Process of a Magnetic Island by Forced Reconnection*; Mar. 1991

NIFS-81 K. Takahata, N. Yanagi, T. Mito, J. Yamamoto, O.Motojima and LHDDesign Group, K. Nakamoto, S. Mizukami, K. Kitamura, Y. Wachi, H. Shinohara, K. Yamamoto, M. Shibui, T. Uchida and K. Nakayama, *Design and Fabrication of Forced-Flow Coils as R&D Program for Large Helical Device*; Mar. 1991

NIFS-82 T. Aoki and T. Yabe, *Multi-dimensional Cubic Interpolation for ICF Hydrodynamics Simulation*; Apr. 1991

NIFS-83 K. Ida, S.-I. Itoh, K. Itoh, S. Hidekuma, Y. Miura, H. Kawashima, M. Mori, T. Matsuda, N. Suzuki, H. Tamai, T.Yamauchi and JFT-2M Group, *Density Peaking in the JFT-2M Tokamak Plasma with Counter Neutral Beam Injection* ; May 1991

NIFS-84 A. Iiyoshi, *Development of the Stellarator/Heliotron Research*; May 1991

NIFS-85 Y. Okabe, M. Sasao, H. Yamaoka, M. Wada and J. Fujita, *Dependence of Au^- Production upon the Target Work Function in a Plasma-Sputter-Type Negative Ion Source;* May 1991

NIFS-86 N. Nakajima and M. Okamoto, *Geometrical Effects of the Magnetic Field on the Neoclassical Flow, Current and Rotation in General Toroidal Systems*; May 1991

NIFS-87 S. -I. Itoh, K. Itoh, A. Fukuyama, Y. Miura and JFT-2M Group, *ELMy-H mode as Limit Cycle and Chaotic Oscillations in Tokamak Plasmas;* May 1991

NIFS-88 N.Matsunami and K.Kitoh, *High Resolution Spectroscopy of H^+ Energy Loss in Thin Carbon Film;* May 1991

NIFS-89 H. Sugama, N. Nakajima and M.Wakatani, *Nonlinear Behavior of Multiple-Helicity Resistive Interchange Modes near Marginally Stable States;* May 1991

NIFS-90 H. Hojo and T.Hatori, *Radial Transport Induced by Rotating RF Fields and Breakdown of Intrinsic Ambipolarity in a Magnetic Mirror*; May 1991

NIFS-91 M. Tanaka, S. Murakami, H. Takamaru and T.Sato, *Macroscale Implicit, Electromagnetic Particle Simulation of Inhomogeneous and Magnetized Plasmas in Multi-Dimensions;* May 1991

NIFS-92 S. - I. Itoh, *H-mode Physics, -Experimental Observations and Model Theories-, Lecture Notes, Spring College on Plasma Physics, May 27 - June 21 1991 at International Centre for Theoretical Physics (IAEA UNESCO) Trieste, Italy ;* Jun. 1991

NIFS-93 Y. Miura, K. Itoh, S. - I. Itoh, T. Takizuka, H. Tamai, T. Matsuda, N. Suzuki, M. Mori, H. Maeda and O. Kardaun, *Geometric Dependence of the Scaling Law on the Energy Confinement Time in H-mode Discharges;* Jun. 1991

NIFS-94 H. Sanuki, K. Itoh, K. Ida and S. - I. Itoh, *On Radial Electric Field Structure in CHS Torsatron / Heliotron;* Jun. 1991

NIFS-95 K. Itoh, H. Sanuki and S. - I. Itoh, *Influence of Fast Ion Loss on Radial Electric Field in Wendelstein VII-A Stellarator;* Jun. 1991

NIFS-96 S. - I. Itoh, K. Itoh, A. Fukuyama, *ELMy-H mode as Limit Cycle and Chaotic Oscillations in Tokamak Plasmas;* Jun. 1991

NIFS-97 K. Itoh, S. - I. Itoh, H. Sanuki, A. Fukuyama, *An H-mode-Like Bifurcation in Core Plasma of Stellarators;* Jun. 1991

NIFS-98 H. Hojo, T. Watanabe, M. Inutake, M. Ichimura and S. Miyoshi, *Axial Pressure Profile Effects on Flute Interchange Stability in the Tandem Mirror GAMMA 10;* Jun. 1991

NIFS-99 A. Usadi, A. Kageyama, K. Watanabe and T. Sato, *A Global Simulation of the Magnetosphere with a Long Tail : Southward and Northward IMF;* Jun. 1991

NIFS-100 H. Hojo, T. Ogawa and M. Kono, *Fluid Description of Ponderomotive Force Compatible with the Kinetic One in a Warm Plasma* ; July 1991

NIFS-101 H. Momota, A. Ishida, Y. Kohzaki, G. H. Miley, S. Ohi, M. Ohnishi K. Yoshikawa, K. Sato, L. C. Steinhauer, Y. Tomita and M. Tuszewski *Conceptual Design of D-^{3}He FRC Reactor "ARTEMIS"* ; July 1991

NIFS-102 N. Nakajima and M. Okamoto, *Rotations of Bulk Ions and Impurities in Non-Axisymmetric Toroidal Systems* ; July 1991

NIFS-103 A. J. Lichtenberg, K. Itoh, S. - I. Itoh and A. Fukuyama, *The Role of Stochasticity in Sawtooth Oscillation* ; Aug. 1991

NIFS-104 K. Yamazaki and T. Amano, *Plasma Transport Simulation Modeling for Helical Confinement Systems;* Aug. 1991

NIFS-105 T. Sato, T. Hayashi, K. Watanabe, R. Horiuchi, M. Tanaka, N. Sawairi and K. Kusano, *Role of Compressibility on Driven Magnetic Reconnection ;* Aug. 1991

NIFS-106 Qian Wen - Jia, Duan Yun - Bo, Wang Rong - Long and H. Narumi, *Electron Impact Excitation of Positive Ions - Partial Wave Approach in Coulomb - Eikonal Approximation* ; Sep. 1991

NIFS-107 S. Murakami and T. Sato, *Macroscale Particle Simulation of Externally Driven Magnetic Reconnection;* Sep. 1991